DR ALISDAIR FERNIE (Orcid ID : 0000-0001-9000-335X)
PROF. MANUEL RODRIGUEZ-CONCEPCION (Orcid ID : 0000-0002-1280-2305)

Article type : - Regular Manuscript

Several geranylgeranyl diphosphate synthase isoforms supply metabolic substrates for carotenoid biosynthesis in tomato

M. Victoria BARJA[1,a], Miguel EZQUERRO[1,a], Stefano BERETTA[1], Gianfranco DIRETTO[2], Igor FLOREZ-SARASA[1], Elisenda FEIXES[1], Alessia FIORE[2], Rumyana KARLOVA[3], Alisdair R. FERNIE[4], Jules BEEKWILDER[5], Manuel RODRIGUEZ-CONCEPCION[1,6,*]

1 Centre for Research in Agricultural Genomics (CRAG) CSIC-IRTA-UAB-UB, Campus UAB Bellaterra, 08193 Barcelona, Spain.

2 Italian National Agency for New Technologies, Energy, and Sustainable Development, Casaccia Research Centre, 00123 Rome, Italy.

3 Laboratory of Plant Physiology, Wageningen University and Research, 6700AA Wageningen, The Netherlands.

4 Max-Planck-Institut für Molekulare Pflanzenphysiologie, 14476 Potsdam-Golm, Germany.

5 BU Bioscience, Wageningen University and Research, 6700AA Wageningen, The Netherlands

6 Institute for Plant Molecular and Cell Biology (IBMCP), CSIC-Universitat Politècnica de València, 46022 Valencia, Spain.

a, These authors equally contributed to the work.

(*) Corresponding author:
Manuel RODRIGUEZ-CONCEPCION, **Email**: manuelrc@ibmcp.upv.es

ORCID numbers:
M. Victoria BARJA: 0000-0002-3846-4885
Miguel EZQUERRO: 0000-0002-3051-5502
Stefano BERETTA: none yet
Gianfranco DIRETTO: 0000-0002-1441-0233
Igor FLOREZ-SARASA: 0000-0002-1862-7931
Elisenda FEIXES: 0000-0003-0285-1979
Alessia FIORE: none yet
Rumyana KARLOVA: 0000-0003-0230-6428
Alisdair R. FERNIE: 0000-0001-9000-335X
Jules BEEKWILDER: 0000-0003-3238-4427
Manuel RODRIGUEZ-CONCEPCION: 0000-0002-1280-2305

Received: *22 July 2020*
Accepted: *8 February 2021*

SUMMARY

- Geranylgeranyl diphosphate (GGPP) produced by GGPP synthase (GGPPS) serves as a precursor for many plastidial isoprenoids, including carotenoids. Phytoene synthase (PSY) converts GGPP into phytoene, the first committed intermediate of the carotenoid pathway.
- Here we used biochemical, molecular, and genetic tools to characterize the plastidial members of the GGPPS family in tomato (*Solanum lycopersicum*) and their interaction with PSY isoforms.
- The three tomato GGPPS isoforms found to localize in plastids (SlG1, 2 and 3) exhibit similar kinetic parameters. Gene expression analyses showed a preferential association of individual GGPPS and PSY isoforms when carotenoid biosynthesis was induced during root mycorrhization, seedling deetiolation and fruit ripening. SlG2, but not SlG3, physically interacts with PSY proteins. By contrast, CRISPR-Cas9 mutants defective in SlG3 showed a stronger impact on carotenoid levels and derived metabolic, physiological and developmental phenotypes than those impaired in SlG2. Double mutants defective in both genes could not be rescued.
- Our work demonstrates that the bulk of GGPP production in tomato chloroplasts and chromoplasts relies on two cooperating GGPPS paralogs, unlike other plant species such as *Arabidopsis thaliana*, rice or pepper, which produce their essential plastidial isoprenoids using a single GGPPS isoform.

KEYWORDS

carotenoids, geranylgeranyl diphosphate (GGPP), prenyltransferase, ripening, synthase, tomato

INTRODUCTION

Isoprenoids are essential biological molecules in all living organisms. In particular, plants are the main source of the enormous structural and functional variety that characterizes this family of compounds (Pulido et al., 2012; Tholl, 2015). The building blocks for the biosynthesis of all isoprenoids are isopentenyl diphosphate (IPP) and its double-bond isomer dimethylallyl diphosphate (DMAPP). These five-carbon (C5) universal isoprenoid units are produced in plants by the mevalonic acid (MVA) pathway in the cytosol and the methylerythritol 4-phosphate (MEP) pathway in plastids (Vranová et al., 2013; Rodríguez-Concepción and Boronat, 2015). Short-chain prenyltransferases subsequently condense one or more molecules of IPP to one molecule of DMAPP giving rise to C10, C15, C20 and C25 prenyl diphosphates known as geranyl diphosphate (GPP), farnesyl diphosphate (FPP), geranylgeranyl diphosphate (GGPP), and geranylfarnesyl diphosphate (GFPP), respectively. These molecules are the immediate precursors for downstream pathways leading to the production of the main groups of isoprenoids.

Carotenoids are one of the most studied groups of plant isoprenoids. These C40 tetraterpenes are greatly demanded by cosmetic and agro-food industries as natural red to yellow pigments and provide benefits for human health, *e.g.* as precursors of vitamin A and other biologically active molecules (Sandmann, 2015; Rodriguez-Concepcion et al., 2018). In plants, carotenoids have different functions. In photosynthetic tissues, they are required for the assembly of the photosynthetic apparatus, contribute to light harvesting and are essential for photoprotection by dissipating excess light energy as heat and by scavenging reactive oxygen species. They are also fundamental in growth regulation, since they are the precursors of retrograde signals and phytohormones such as abscisic acid (ABA) and strigolactones. As a secondary role, carotenoids provide distinctive colors to flowers and fruits to attract pollinators and seed dispersal animals (Nisar et al., 2015; Yuan et al., 2015). In plants, carotenoids are produced and stored in plastids, including chloroplasts and chromoplasts (Ruiz-Sola and Rodríguez-Concepción, 2012; Sun et al., 2018). MEP-derived IPP and DMAPP are converted into GGPP by plastidial GGPP synthase (GGPPS) isoforms and then GGPP is transformed into phytoene by phytoene synthase (PSY) enzymes. The production of phytoene, the first committed intermediate of the carotenoid pathway, is considered to be a major rate-determining step regulating the metabolic flux through this pathway (Fraser et al., 2002). In tomato (*Solanum lycopersicum*), three PSY-encoding genes control carotenoid biosynthesis in different tissues. *PSY1* expression is boosted during ripening to produce carotenoids involved in the pigmentation of the fruit (Bartley et al., 1992; Fray and Grierson, 1993; Giorio et al., 2008; Kachanovsky et al., 2012). *PSY2* is expressed in all tissues, including fruits, but transcript levels are much higher than those of *PSY1* in photosynthetic

tissues, where carotenoids are required for photosynthesis and photoprotection (Bartley and Scolnik, 1993; Giorio et al., 2008). Lastly, *PSY3* is mainly expressed in roots and it is induced during mycorrhization (Walter et al., 2015; Stauder et al., 2018), when carotenoid biosynthesis is up-regulated to produce strigolactones and apocarotenoid molecules essential for the establishment of the symbiosis (Fester et al., 2002, 2005; Baslam et al., 2013; Ruiz-Lozano et al., 2016; Stauder et al., 2018). Whether the corresponding PSY isoforms use GGPP supplied by different GGPPS isoforms remains unknown.

Several GGPP synthase (GGPPS) paralogs have been retained in plants during evolution (Beck et al., 2013; Zhang et al., 2015; Ruiz-Sola et al., 2016a, 2016b; Zhou et al., 2017; Wang et al., 2018). However, a single GGPPS isoform appears to produce the GGPP substrate needed for the production of carotenoids and other plastidial isoprenoids in the three plant species whose GGPPS families have been best characterized to date: *Arabidopsis thaliana,* rice (*Oryza sativa*) and pepper (*Capsicum annuum*) (Ruiz-Sola et al., 2016a, 2016b; Zhou et al., 2017; Wang et al., 2018). While tomato has become one of the best plant systems to study the biosynthesis of carotenoids and its regulation, we still have an incomplete picture of the GGPPS family in this plant. Recent work has determined that five genes encoding GGPPS homologs exist in the tomato genome, three of which were confirmed to produce GGPP *in vitro* and localize in plastids (Zhou and Pichersky, 2020). Which of these plastidial GGPPS isoforms are required for the production of carotenoids in photosynthetic tissues (*e.g.* for photoprotection), fruits (*e.g.* for pigmentation) or roots (*e.g.* for mycorrhization) remains unknown. Here we characterized the *in vivo* role of these plastidial GGPPS enzymes and provide clues to understand how the supply of plastidial GGPP for the synthesis of carotenoids with different biological functions in particular tomato tissues is regulated in this important crop plant.

MATERIALS AND METHODS

Plant material

Tomato (*Solanum lycopersicum* var. MicroTom) plants were used for most experiments. Seed germination, plant growth and sample collection were carried out as described (Method S1). *A. tumefaciens* GV3101 strain was used to stably transform tomato MicroTom cotyledons with plasmids harboring two sgRNAs to disrupt *SlG2* and *SlG3* genomic sequences as described (Fernandez et al., 2009). The sgRNAs were designed for each gene to create short deletions using the CRISPR P 2.0 online tool (http://crispr.hzau.edu.cn/CRISPR2/) (Liu et al., 2017). The cloning of the sgRNA sequences was performed as described (Schiml et al., 2016) using a pDE-

Cas9 plasmid providing kanamycin resistance (Method S2). Primers and cloning steps are detailed in Tables S1 and S2, respectively. *In vitro* regenerated T1 lines were identified based on kanamycin resistance (100 µg/ml), PCR genotyping and restriction analyses. Homozygous T2 lines lacking Cas9 were obtained after segregation. Stable T3 offspring was used for further experiments. Method S2 and Tables S1 and S2 describe the generation of the rest of the constructs. *Nicotiana benthamiana* plants were grown and used for transient expression assays (agroinfiltration) as previously described (Llorente et al., 2020).

Gene Co-expression Network (GCN) analyses

GCN analyses were performed as previously described (Ahrazem et al., 2018). Pairwise Pearson correlations between each GGPPS gene and each selected isoprenoid biosynthetic input gene were computed for leaf and fruit tissues throughout their development and Fisher's Z-transformation was used to test their statistical significance.

RNA analyses

RNA isolation, cDNA synthesis, and RT-qPCR analyses were carried out as described (Method S3). Normalized transcript abundances were calculated as described previously (Simon, 2003) using tomato *ACT4* (*Solyc04g011500*) or *EXP* (*Solyc07g025390*) as endogenous reference genes. Three biological replicates of cDNA samples from roots of non-mycorrhized and mycorrhized tomato plants (Ruiz-Lozano et al., 2016) were kindly provided by Dr. Juan Antonio López-Ráez.

Protein analyses

In vitro GGPPS activity determination was performed as described (Method S4). Purified enzymes were used to calculate kinetic parameters as described (Barja and Rodríguez-Concepción, 2020). Protein concentration was determined according to Bradford method (Bradford, 1976). GGPPS activity assays in *E. coli* were carried out as described (Beck et al., 2013). Subcellular localization assays were performed by *Agrobacterium tumefaciens*-mediated transient expression in *N. benthamiana* leaves (Sparkes et al., 2006). Leaves were co-infiltrated with strains carrying appropriate constructs (Method S2) and a HC-Pro silencing suppressor (Goytia et al., 2006) as described (Method S5). Subcellular localization of GFP fusion proteins was determined three days post-infiltration with an Olympus FV 1000 confocal laser-scanning

microscope (Method S5). Co-immunoprecipitation (Co-IP) assays were performed in *N. benthamiana leaves* as described (Muñoz and Castellano, 2018) (Method S6). Immunoblot analyses was performed as described (Pulido et al., 2013).

Metabolite analysis

Detection of prenyl diphosphates was carried out as described (Ruiz-Sola et al., 2016b). Carotenoids, chlorophylls and tocopherols were extracted as described (Method S7). Separation and detection was next performed using an Agilent 1200 series HPLC system (Agilent Technologies) as previously reported (Fraser et al., 2000). ABA levels were determined as described (Diretto et al., 2020). Primary metabolites were extracted, annotated and quantified as described (Llorente et al., 2020).

RESULTS

SlG1, SlG2 and SlG3 are GGPP-producing plastidial enzymes with similar kinetic properties.

Several genes encoding proteins with homology to GGPPS enzymes are found in the tomato genome (Ament et al., 2006; Fraser et al., 2007; Stauder et al., 2018; Zhou and Pichersky, 2020). From these, three have been found to localize in plastids and produce GGPP *in vitro*, namely *GGPPS1* (*Solyc11g011240*), *GGPPS2* (*Solyc04g079960*) and *GGPPS3* (*Solyc02g085700*), herein referred to as *SlG1*, *SlG2* and *SlG3* (Table S3). We confirmed the plastidial targeting of these three isoforms by expressing constructs encoding GFP fusions of the full-length SlG1-3 proteins in agroinfiltrated tobacco (*Nicotiana benthamiana*) leaves. In all three cases, fluorescence corresponding to the GFP fusion proteins co-localized with chlorophyll autofluorescence (Figure S1), supporting the conclusion that they are all efficiently targeted to chloroplasts. We also experimentally confirmed the ability of purified SlG1-3 proteins to produce GGPP *in vitro*. The three tomato isoforms were expressed in *Escherichia coli* cells without their predicted plastid-targeting sequences (Figure S2) and whole-cell protein extracts were directly used for activity assays in the presence of IPP and DMAPP followed by the analysis of the reaction products by LC-MS (Figure S3). As positive and negative controls, we used the Arabidopsis AtG11 (active) and AtG11s (inactive) proteins (Ruiz-Sola et al., 2016b). This experiment confirmed that SlG1, SlG2, SlG3 and AtG11 (but no AtG11s) produced only GGPP (Figure S3A), in agreement with recently reported data (Zhou and Pichersky, 2020). To gain new knowledge on the biochemical properties of these enzymes, we used purified proteins to

calculate their kinetic parameters. Enzymatic assays performed as described (Barja and Rodríguez-Concepción, 2020) showed that all tested GGPPS proteins exhibited a similar optimal pH around 7.5 (Figure S3B), as expected for stromal enzymes (Höhner et al., 2016). The parameters Km (an estimator of the apparent affinity for the IPP and DMAPP substrates) and Vmax exhibited very similar values among the three tomato enzymes (Table 1). They are also similar to those obtained for AtG11 here and elsewhere (Wang and Dixon, 2009; Camagna et al., 2019). We therefore conclude that tomato SlG1, SlG2 and SlG3 and Arabidopsis AtG11 are plastidial GGPPS enzymes with very similar kinetic properties.

Gene expression profiles suggest a major role of SlG2 and SlG3 in chloroplasts and chromoplasts

Analysis of public gene expression databases showed that the genes encoding SlG1-3 enzymes were expressed in roots, leaves and flowers (Figure S4). Of these, the most highly expressed gene is *SlG3* followed by *SlG2*, while *SlG1* transcripts are present at very low levels. *SlG2* and *SlG3*, but not *SlG1,* are also expressed at high levels in fruit pericarp and seed tissues (Figure S4). As an initial approach to get an insight on the possible functions of these individual isoforms, we performed a gene co-expression network (GCN) analysis. This is a powerful tool to infer biological functions that we previously used to identify AtG11 as the main GGPPS isoform for plastidial isoprenoid production in Arabidopsis (Ruiz-Sola et al., 2016a). By using publicly available databases for plant comparative genomics (*PLAZA 4.0*, *Phytozome*), we searched for tomato homologs of the plastidial pathways that supply GGPPS substrates (MEP pathway) and consume GGPP to produce carotenoids, chlorophylls, tocopherols, phylloquinone, plastoquinone, gibberellins, strigolactones and ABA (Table S4). We retrieved their expression data from *TomExpress* (Zouine et al., 2017) experiments carried out using either leaf or fruit samples at different developmental stages (Table S5). Then, we calculated their correlation with *SlG1, SlG2* and *SlG3* expression using pairwise Pearson correlations. The results of the GCN analyses are shown in Figure 1 and Figure S5, and correlations are listed in Table S6. It was not possible to obtain correlation data for tomato roots since only two experiments using root samples are deposited in the *TomExpress* database. In leaves and fruits, *SlG1* was poorly co-expressed with the query genes. By contrast, and similar to that observed with *AtG11* (Ruiz-Sola et al., 2016a)*, SlG2* and, to a lower extent, *SlG3* were highly connected to plastidial isoprenoid biosynthetic genes in leaf tissues. Connectivity was lower in fruit, and in this case it was a bit higher for *SlG3* (Figure 3). These results suggest that SlG2 and SlG3 might be the main GGPP-producing isoforms in leaf chloroplasts and fruit chromoplasts.

In tomato, carotenoids contribute to mycorrhizal associations, photoprotection, and fruit pigmentation and, hence, the levels of these GGPP-derived metabolites increase during root mycorrhization, seedling de-etiolation, and fruit ripening. In agreement with the rate-determining role of PSY for carotenoid synthesis (Fraser et al., 2002), the expression levels of PSY-encoding genes also increase during such carotenoid-demanding developmental processes. By using real-time quantitative PCR (qPCR) analysis, we experimentally confirmed the up-regulation of *PSY1* during fruit ripening and *PSY3* in mycorrhized roots (Figure 2). Furthermore, we found that the *PSY2* gene was more strongly upregulated than *PSY1* during tomato seedling de-etiolation (Figure 2). Using the same samples, we observed that only *SlG1* was upregulated during root mycorrhization, similarly to the expression pattern observed for *PSY3* (Figure 2). During fruit ripening, *SlG2* and, to a lower extent, *SlG3* were up-regulated, but not as much as *PSY1* (Figure 2). *SlG2* was also the most strongly upregulated GGPPS-encoding gene during seedling de-etiolation, paralleling *PSY2* induction. Interestingly, *SlG3* and *PSY1* were also induced with a similar profile during this process, even though induction levels were much lower than those observed for *SlG2* and *PSY2* (Figure 2). Together, these data suggest that SlG1 might provide GGPP for PSY3 to produce carotenoids in roots, particularly when needed during mycorrhization, whereas both SlG2 and SlG3 would be required in leaves and fruits to support carotenoid production for photosynthesis (mostly via PSY2) and fruit pigmentation (via PSY1).

SlG2, but not SlG3, can interact with PSY1 and PSY2

A coordinated role for SlG1 and PSY3 in mycorrhization has been already proposed (Stauder et al., 2018) but the possible connection between the other plastidial GGPPS and PSY isoforms remains unclear. GGPPS proteins can physically interact with PSY and other enzymes catalyzing both upstream and downstream biosynthetic steps in the plastids of different plant species (Dogbo and Camara, 1987; Camara, 1993; Maudinas et al., 1977; Fraser et al., 2000; Ruiz-Sola et al., 2016a; Zhou et al., 2017; Camagna et al., 2019; Wang et al., 2018). This mechanism may facilitate channeling of precursors towards specific groups of plastidial isoprenoids. Protein complexes containing both GGPPS and PSY enzymes were isolated from tomato chloroplasts and fruit chromoplasts (Maudinas et al., 1977; Fraser et al., 2000), but the specific isoforms forming these protein complexes were never identified. Given the co-regulation of *SlG2* and *SlG3* with *PSY1* and *PSY2* genes in chloroplasts (i.e. photosynthetic tissues) and chromoplasts (i.e. fruits), we decided to test possible interactions of these isoforms in co-immunoprecipitation assays (Figure 3). Constructs harboring C-terminal Myc-tagged GGPPS and HA-tagged PSY sequences were combined and transiently co-expressed in *N. benthamiana* leaves. As negative

control, we used a Myc-tagged version of Arabidopsis phosphoribulokinase (PRK-Myc), a stromal enzyme of the Calvin cycle. Both PSY1-HA and PSY2-HA could be co-immunoprecipitated with SlG2-Myc, suggesting that they are present in the same complexes *in vivo* (Figure 3). By contrast, none of these PSY isoforms could be detected in the samples co-immunoprecipitated with either SlG3-Myc or PRK-Myc. The same Myc-tagged SlG2 and SlG3 proteins used in these experiments were able to co-immunoprecipitate their HA-tagged counterparts (Figure 3). This result, consistent with the ability of GGPPS proteins to form homodimers and also heterodimers, confirms that the observed lack of interaction of SlG3 with PSY enzymes was not due to SlG3-Myc having lost its capacity to interact with other proteins.

Loss of function mutants defective in SlG3, but not those impaired in SlG2, show lower levels of photosynthetic pigments and activity

To further explore the biological roles of SlG2 and SlG3, we generated CRISPR-Cas9 mutants defective in these enzymes (Figure 4). We designed two single guide RNAs (sgRNA) for each gene with the aim of creating deletions encompassing unique restriction sites for rapid screening (Figure 4A). Two independent deletion alleles that created premature translation stop codons were selected for each gene and named *slg2-1*, *slg2-2*, *slg3-1* and *slg3-2* (Figure 4A) (Figures S6-S8). To confirm that the truncated proteins lacked GGPPS activity, we tested them in *E. coli* strains that synthesize the red carotenoid lycopene only when a source of GGPP is supplied (Ruiz-Sola et al., 2016b). Transformation with constructs harboring the mutant enzymes did not produce more lycopene than empty plasmid controls, indicating that they lack GGPPS activity. (Figure 4B). Once confirmed that the selected mutant alleles produced non-functional proteins, homozygous lines without Cas9 were obtained and used for further experiments.

The most obvious phenotype among the selected lines was the pale color of *slg3* mutants compared to *slg2* alleles or azygous (WT) plants (Figure 5). This phenotype was clear in emerging and young leaves but it weakened as leaves grew and became mature (Figure 5A). The pale color correlated with significantly reduced levels of carotenoids and chlorophylls in young leaves of *sgl3-1* and *sgl3-2* lines compared to those of WT plants (Figure 5B) (Table S7). The differences were less clear in the case of tocopherols, another group of GGPP-derived plastidial isoprenoids (Figure 5B). Similar levels of carotenoids, chlorophylls and tocopherols were detected in mature leaves of WT, *slg2* and *slg3* plants (Figure 5B) (Table S7). To test whether the reduced accumulation of photosynthesis-related isoprenoids in *slg3* lines had an impact on photosynthesis, we quantified effective quantum yield of photosystem II (ϕPSII) in both

young and mature leaves (Figure 5C). A 30% reduction in ϕPSII was observed in young leaves from *slg3* plants compared to those of WT or *slg2* lines, consistent with the *slg3*-specific reduction of GGPP-derived metabolites. Despite similar levels of photosynthetic pigments accumulated in the mature leaves of all genotypes tested, ϕPSII was slightly reduced in some mutants relative to WT lines (Figure 5C).

We further explored possible effects that the loss of SlG2 or SlG3 function might have on other metabolic pathways using the same samples of young leaves used for isoprenoid and ϕPSII determination (Figure 6). GC-MS metabolite profiling showed strongly decreased levels of sucrose, glucose and fructose in SlG3-defective leaves, likely due to photosynthetic impairment. Mutant *slg3* leaves also displayed increased levels of amino acids derived from glycerate (Ser and Gly), shikimate (Phe, Trp and Tyr), pyruvate (Val, Ile and Ala), 2-oxoglutarate (Glu, Orn, His and GABA) and malate (Asp, Asn, Lys, Thr, Met, homoserine and beta-alanine). In line with some of these amino acid changes, SlG3-defective leaves displayed altered accumulation of tricarboxylic acid cycle-related intermediates (citrate and 2-oxoglutarate). Only a few common changes were detected in both *slg2* and *slg3* leaves. They included a decrease in putrescine and ascorbate levels (more pronounced in *slg3* leaves), as well as an altered accumulation of metabolites produced by the plastidial shikimate pathway, including the above mentioned aromatic amino acids and phenylpropanoid derivatives such as caffeate and 3-caffeoyl-quinate (Figure 6). The levels of the carotenoid-derived hormone ABA were similar in WT and mutant samples (Figure 6 and Table 2).

Ripening-associated fruit pigmentation is altered in *slg2* and *slg3* mutants in correlation with their carotenoid profile

Lines with reduced levels of plastidial GGPPS activity also showed alterations in reproductive development (Figure 7). Flowering time was similar in WT, *slg2* and *slg3* plants (Figure 7A). However, pigmentation changes associated to fruit ripening were visually delayed in mutant fruits (Figure 7B). Tomato fruits reach their final size at the mature green (MG) stage and then start to ripe. The first visual symptoms of ripening define the breaker (B) stage, when chlorophyll degradation and carotenoid biosynthesis change the fruit color from green to yellow (Figure 7C). As ripening advances, accumulation of orange and red carotenoids (β-carotene and lycopene, respectively) progressively change the fruit color and define the orange (O) and eventually red (R) stages (Figure 7C). The time from anthesis to B was similar in WT and SlG2-defective fruits but it was longer in the *slg3* mutants (Figure 7B) (Figure S9). Fruits from lines defective in SlG3,

but also those defective in SlG2, showed a pigmentation delay in the transition from B to O. The delay was observed both on-vine (i.e. in fruits attached to the plant) and off-vine (i.e. in fruits detached from the plant at the B stage) (Figure 7B) (Figure S9). Both on-vine and off-vine measurements revealed that *slg2* mutants also took longer to reach the R stage compared to WT fruits (Figure S9), whereas *slg3* mutants did not reach a proper R stage as they developed a dark-orange color when ripe and never turned fully red (Figure 7C).

WT and mutant fruits showed similar levels of carotenoids, chlorophylls and tocopherols at the MG stage (Figure S10), but clear differences were detected in ripe fruits at B+10, i.e. 10 days after B (Figures 6 and 7D) (Table S7). Phytoene and lycopene were decreased in all mutants, although the impact was higher in the case of *slg3* fruits. No significant differences were found for β-carotene, although the levels of this orange carotenoid tended to be higher in *slg3* mutants. This, together with the lower levels of the red carotenoid lycopene may explain the dark orange color of B+10 *slg3* fruits (Figure 7C). Tocopherols also showed a trend towards higher abundance in SlG3-deficient fruits, a change that was statistically significant in the *slg3-1* allele (Figure 7D) or when *slg3-1* and *slg3-2* samples were considered together (Figure 6).

Unlike that observed in young leaves, ABA levels were reduced in B+10 fruits of *slg2* and, most strongly, *slg3* mutants compared to WT controls (Figure 6 and Table 2). At the level of primary metabolites, B+10 fruits from both *slg2* and *slg3* mutants exhibited increased levels of raffinose, galacturonate, pyruvate and Asp, and lower levels of Ser, Gly, Tyr, Val, Ala, Glu and GABA than WT controls (Figure 6). The changes in these metabolites were typically stronger in the case of *slg3* fruits, paralleling that observed for carotenoids and derived ABA levels.

Double mutants defective in both SlG2 and SlG3 are not viable

To assess the impact of simultaneous disruption of both *SlG2* and *SlG3* genes, alleles *slg2-2* and *slg3-1* were crossed using the former as female parent and the latter as male parent or vice versa. Double heterozygous F1 plants from each cross were allowed to self-pollinate and the resulting seeds were used to screen the F2 population for double homozygous plants, which were expected to occur at a Mendelian frequency of 6.25% (1 in 16). We performed two rounds of screening. In the first one, 200 seeds (100 from each cross) were plated and all of them germinated and produced green seedlings. In the second round, carried out with older seeds, 80 seeds were plated and 76 (95%) germinated (Table 3). The seeds that failed to germinate (4) were manually open and found to contain either albino/pale (3) or green (1) embryos (Figure S11). PCR genotyping of these embryos (Figure S11) and of the remaining 276 seedling did not

identify double homozygous mutants (Table 3). A chi-squared goodness of fit test performed with 8 degrees of freedom and 95% interval of confidence confirmed that the observed genotype frequencies did not follow the expected Mendelian segregation in any of the two experiments or when considering all data together (Table 3). Besides the absence of double *slg2-2 slg3-1* mutants (herein referred to as *g2g2 g3g3*), lines with one of the two genes in homozygosis and the second one in heterozygosis (i.e *g2g2 G3g3* and *G2g2 g3g3*) were found at lower frequencies than predicted (Table 3), suggesting a gene dosage effect. Our interpretation of these results is that the absence of both *SlG2* and *SlG3* results in a lethal phenotype that is partially rescued by incorporating one copy of any of these two genes (as in *g2g2 G3g3* or *G2g2 g3g3* plants) and fully rescued when two copies are present in the genome (as in double heterozygous or single homozygous mutants). These results, together with the similar expression levels of both genes in developing tomato seeds (Figure S4), suggest that SlG2 and SlG3 contribute similarly and additively to embryo or/and seed development.

The phenotypes of single *slg3* mutants are exacerbated in lines with the *SlG2* gene in heterozygosis.

Plants segregating from double heterozygous F1 plants (*G2g2 G3g3*) that showed a single mutant genotype (i.e *g2g2 G3G3* and *G2G2 g3g3*) or one of the two genes in homozygosis and the second one in heterozygosis (i.e *g2g2 G3g3* and *G2g2 g3g3*) were transferred to soil and used to carefully examine their phenotype. Consistent with that described for the *slg2-2* and *slg3-1* parentals (Figure 5), young leaves of *g2g2 G3G3* plants showed unchanged pigmentation and WT levels of photosynthetic pigments (chlorophylls and carotenoids) and photosynthetic activity (ϕPSII), whereas those of *G2G2 g3g3* plants were paler and displayed a reduction of photosynthetic pigments and activity (Figure 8). Most interestingly, the phenotypes of the *slg3* mutants were intensified when one of the two genomic copies of *SlG2* was inactivated in the *G2g2 g3g3* line (Figure 8). Loss of a *SlG3* gene copy in the *slg2* mutant background, however, was not sufficient to trigger statistically significant changes in young leaves compared to WT or *slg2* lines. This result indicates that a single copy of the *SlG3* gene is sufficient to provide GGPP for the production of photosynthetic pigments in chloroplasts, even when no SlG2 activity is available. In the case of mature leaves, no significant differences were observed between WT and any of the mutant lines (Figure 8).

At the level of fruit ripening, quantification of fruit color using the TomatoAnalyzer 4.0 tool (Gonzalo et al., 2009) confirmed the pigmentation delay previously observed in single mutants

defective in SlG2 or, to a higher extent, SlG3 (Figure 7) and further showed a stronger effect when one of the two genomic copies of *SlG2* was additionally inactivated in the *slg3* background (Figure 9A). Analysis of the expression of ripening marker genes such as *E8* and *ACS2* (Estornell et al., 2009; Llorente et al., 2016; D'Andrea et al., 2018) showed that the peak of *E8* and *ACS2* expression observed at the onset of ripening (Figure S4) was reduced in the mutants (Figure 9B). Again, the stronger effect was observed in lines without SlG3 activity and tended to be higher in *G2g2 g3g3* compared to *G2G2 g3g3* lines (Figure 9B).

DISCUSSION

The fundamental basis for our knowledge of the regulation of GGPP biosynthesis in plants mainly comes from the characterization of the Arabidopsis GGPPS family (Zhu et al., 1997a, 1997b; Okada et al., 2000; Beck et al., 2013; Nagel et al., 2015; Ruiz-Sola et al., 2016a, 2016b; Wang et al., 2016). In this model plant, there are two plastid-targeted GGPPS paralogs (AtG2 and AtG11) but only AtG11 appears to be required for the production of plastidial isoprenoids (Beck et al., 2013; Nagel et al., 2015; Ruiz-Sola et al., 2016a, 2016b). The gene encoding AtG11 is ubiquitously expressed at high levels and can generate long transcripts encoding the plastid-targeted isoform but also short transcripts encoding a cytosolic enzyme that retains enzymatic activity and is essential for embryo development (Ruiz-Sola et al., 2016b). The production of GGPP has also been studied in a few crop plants (Wang and Dixon, 2009; Zhang et al., 2015; Zhou et al., 2017; Wang et al., 2018, 2019). Similar to Arabidopsis, rice and pepper contain only one enzymatically active GGPPS isoform localized in plastids, named OsGGPPS1 (OsG1 in short) and CaGGPPS1 (CaG1), respectively (Zhou et al., 2017; Wang et al., 2018). Strikingly, only scattered information was available to date on the tomato GGPPS family despite this species being a well-established model plant that accumulates high amounts of GGPP-derived metabolites of human interest such as carotenoids in fruits. Here we demonstrate that, in tomato, two plastidial isoforms (SlG2 and SlG3) coordinately supply GGPP to produce carotenoids and other isoprenoids essential for photosynthesis, fruit pigmentation, and seed viability.

Subfunctionalization of plastidial GGPPS paralogs in tomato might involve several mechanism with a major role for differential gene expression.

The three plastid-targeted GGPPS homologs present in tomato (SlG1-3) produce GGPP with similar kinetic parameters and an optimal pH around 7.5 (Figure S3 and Table 1). Several mechanisms might allow enzymatically similar GGPPS isoforms to acquire new functions,

including (a) localization in distinct subcellular compartments, (b) specific interactions with other protein, and (c) diversification of spatio-temporal gene expression patterns. Despite the clear plastidial localization observed here (Figure S1) and elsewhere (Zhou and Pichersky, 2020) for GFP fusions of the SlG1-3 isoforms, we cannot exclude that shorter extraplastidial versions of these proteins could also be produced *in vivo*, paralleling that observed in the case of AtG11 (Ruiz-Sola et al., 2016b). Indeed, several M residues can be found in the N-terminal region of both SlG2 and SlG3 enzymes (Figure S8); they could be used as alternative translation start sites to produce catalytically active GGPPS enzymes with an absent or shorter (i.e. dysfunctional) plastid-targeting domain.

Besides localization in distinct subcellular compartments, subfunctionalization of GGPPS paralogs might also involve isoform-specific interactions with other proteins. The enzymatic properties of GGPPS proteins change to produce GPP upon heterodimerization with members of the GPP synthase small subunit type I (SSU-I) subfamily (Orlova et al., 2009; Wang and Dixon, 2009). This is what happens upon interaction of SlG1-3 enzymes with the tomato SSU-I protein (Solyc07g064660) (Zhou and Pichersky, 2020). Multienzymatic complexes appear to be particularly important for metabolic channeling of GGPP. In particular, PSY cannot access freely diffusible GGPP or time-displaced GGPP supply by GGPPS (Camagna et al., 2019). Arabidopsis AtG11 and pepper CaG1 can directly interact with PSY proteins (Ruiz-Sola et al., 2016a; Camagna et al., 2019; Wang et al., 2018). We found that tomato SlG2, but not SlG3, is able to interact with PSY1 and PSY2 *in planta* (Figure 3). However, tomato SlG3 might deliver GGPP to PSY enzymes via heterodimerization with PSY-interacting SlG2 (Figure 3). An alternative possibility involves interaction with members of another catalytically-inactive SSU subfamily named type II (SSU-II). Similar to AtG11 and CaG1, OsG1 is the only GGPPS enzyme producing GGPP for carotenoid biosynthesis in rice. Strikingly, OsG1 does not interact with PSY but heterodimerizes with a SSU-II homolog, resulting in its delivery to a large protein complex in thylakoid membranes (Zhou et al., 2017). Interaction with SSU-II proteins was also shown to enhance the GGPP-producing activity of rice OsG1 but also of pepper CaG1 (Wang et al., 2018) and tomato SlG1-3 isoforms (Zhou and Pichersky, 2020). Interestingly, the pepper SSU-II protein also interacts with PSY, suggesting that binding of CaG1 to SSU-II might stimulate both its GGPPS activity and its interaction with PSY (Wang et al., 2018). It is therefore possible that heterodimerization with tomato SSU-II (Solyc09g008920) might also deliver SlG3 to PSY-containing protein complexes and enhance interaction of SlG2 with PSY isoforms.

Regardless of other possible mechanisms discussed above, it appears that a major determinant defining the biological roles of plastidial GGPPS isoforms in tomato is their distinct expression

profiles. Mining of public tomato gene expression databases, GCN analyses and qPCR assays led us to conclude that SlG1 is likely contributing to carotenoid biosynthesis in roots together with PSY3. This conclusion is supported by a recent study showing that the expression of *PSY3* and *SlG1* coordinately responds to tomato root mycorrhization and phosphate starvation (Stauder et al., 2018). The SlG1-PSY3 tandem might be channeling the flux of MEP-derived precursors towards the synthesis of carotenoid-derived molecules that are crucial for the establishment of symbiosis, such as strigolactones and apocarotenoids (Stauder et al., 2018). Unlike *SlG1*, *SlG2* and *SlG3* are constitutively expressed, with *SlG3* being the paralog with the highest expression level in all plant tissues (Figure S4). In leaves, *SlG2* is more strongly co-expressed than *SlG3* with genes from photosynthesis-related isoprenoid pathways (Figure 1). This suggests that the expression of the *SlG2* gene changes more than that of *SlG3* to adapt to conditions requiring a readjustment of the gene expression network regulating the metabolism of isoprenoids such as carotenoids. In agreement, *SlG2* was much more upregulated than *SlG3* during seedling de-etiolation (Figure 2) and leaf development (Figure S4C), when an enhanced production of carotenoids and other photosynthesis-related isoprenoids contributes to assemble a functional photosynthetic machinery. *SlG2* was also much more induced than *SlG3* during fruit ripening, when carotenoid biosynthesis is boosted thanks to the up-regulation of the PSY1 isoform. *PSY1* and *SlG2*, but not *SlG3*, are coordinately regulated by FUL and RIN transcription factors that control the expression of ripening-related genes, including many of the MEP and carotenoid pathways (Fujisawa et al., 2013, 2014).

All these expression data show that *SlG2* expression is more responsive to sudden demands of precursors for the production of isoprenoids, including carotenoids. In contrast, *SlG3* expression is higher and does not change so much, suggesting a house-keeping role to maintain a continuous supply of GGPP in plastids for basal production of carotenoids and other isoprenoids. According to this model, SlG1 and SlG2 would help SlG3 to supply GGPP when a boost in carotenoid production is needed. The very low and restricted expression level of *SlG1*, however, strongly suggests that SlG2 is the main helper isoform for SlG3 in chloroplasts of cotyledons and expanding leaves and chromoplasts of ripening fruit.

GGPPS isoforms SlG2 and SlG3 have functionally interchangeable roles in chloroplasts and chromoplasts.

Analysis of tomato mutants defective in gene copies for SlG2 or/and SlG3 further suggested that these are functionally exchangeable isoforms that participate in the same biological processes.

This might not be obvious when analyzing leaves, as only *slg3* alleles were found to display reduced levels of GGPP-derived isoprenoids and subsequent inhibition of photosynthesis (Figures 5 and 8). However, the effects of reduced isoprenoid synthesis could be indirectly detected in *slg2* leaves too. Thus, our GC-MS analysis showed higher levels of all aromatic amino acids derived from the shikimate pathway (Trp, Tyr and Phe) as well as Phe-derived phenylpropanoids caffeate (caffeic acid) and 3-caffeoyl-quinate (chlorogenic acid) in both *slg2* and *slg3* mutant lines (Figure 6). This might be a physiological response to cope with photooxidative stress caused by lower levels of carotenoids in the mutants, as phenylpropanoids (including Phe-derived flavonoids and anthocyanins) can also function as photoprotective metabolites (Muñoz and Munné-Bosch, 2018). Reduced levels of well-known metabolites associated with oxidative stress such as ascorbate and putrescine in leaves from both mutant lines would also support this view.

Loss of one *SlG3* gene copy in the *slg2* mutant background failed to cause a statistically significant decrease in the levels of photosynthetic pigments or activity, even though a trend towards reduction of chlorophyll and carotenoid levels was observed (Figure 8). However, complete loss of SlG3 activity in lines with one or two functional *SlG2* copies was sufficient to reduce levels of GGPP-derived photoprotective isoprenoids such as carotenoids and tocopherols to an extent that became detectable and impacted photosynthesis (Figure 5), causing sugar starvation and the subsequent metabolic changes observed only in the *slg3* mutant (Figure 6). In agreement, the increased accumulation of most amino acids in *slg3* leaves suggested a high proteolytic activity to generate an alternative respiratory source, a likely response to sugar starvation derived from reduced photosynthesis and/or photooxidative stress (Araújo et al., 2011; Obata and Fernie, 2012; Galili et al., 2016).

The absence of any of the two individual enzymes also decreases plastidial GGPP production in fruit, as deduced from the levels of the main GGPP-derived metabolites (Figure 7D) (Table S7). Tocopherol levels did not decrease in mutant fruit, perhaps because they are mostly produced by recycling the phytyl chain released from the chlorophylls degraded during fruit ripening. By contrast, lycopene (by far the most abundant carotenoid in ripe fruit) and, to a lower extent, phytoene, showed reduced levels in both mutants (Figure 7D) (Table S7). Similar to that observed in leaves, the impact is stronger in *slg3* mutants, consistent with the higher expression levels of the *SlG3* compared to *SlG2* in young leaves and MG fruits (Figure S4). While altered levels of 3-caffeoyl-quinate and citrate were detected only in fruit of the *slg3* mutant, the rest of metabolic changes were similar in *slg2* and *slg3* lines (Figure 6), again supporting the conclusion that these enzymes are redundant and interchangeable. In particular, both *slg2* and *slg3* fruit

showed pigmentation defects associated with a decreased carotenoid accumulation (Figures 7 and 9A). Because ABA is synthesized from carotenoids, its reduced levels in GGPPS-defective ripe fruits but not in leaves (Table 2) may be the result of a more substantial reduction in carotenoid contents in mutant fruit (Figure 7) compared to leaves (Figure 5) (Table S7). A role for ABA in promoting tomato fruit ripening has been proposed based on the analysis of mutants or external application of hormones and inhibitors. This, together with the observed down-regulation of ethylene-related ripening marker genes (*E8* and *ACS2*) in GGPPS-defective fruit (Figure 9B) allows to speculate that reduced ABA levels in the mutant fruit may contribute to delay ripening either directly or indirectly via ethylene (Zhang et al., 2009; McQuinn et al., 2020). Additionally, metabolic roles of SlG2 and SlG3 besides their GGPPS activity in plastids might play a role in fruits but also in developing seeds, hence explaining why we could not isolate a double *slg2 slg3* mutant (Table 3). The observation that the lethal phenotype is dose-dependent in an isoform-independent fashion (i.e. can be rescued by a single genomic copy of either *SlG2* or *SlG3*) reinforces our conclusion that SlG2 and SlG3 have functionally interchangeable roles.

Concluding remarks.

Retention of multiple gene copies after duplication events may allow the acquisition of new functions (neofunctionalization) or partitioning the ancestral functions between duplicate partners (subfunctionalization), via evolution of coding sequence and/or regulatory regions. The work reported here demonstrates that the bulk of GGPP production in tomato leaf chloroplasts and fruit chromoplasts relies on two redundant but cooperating GGPPS paralogs, SlG2 and SlG3. Additionally, the SlG1 isoform might contribute to GGPP synthesis in root plastids. This subfunctionalization scenario contrasts with that described to date in other plant species such as *Arabidopsis*, rice or pepper, which produce their essential plastidial isoprenoids using a single GGPPS isoform. However, it is likely that tomato is not an exception. Examples of gene families encoding enzyme isoforms located in the same cell compartment but differing in gene expression profiles abound in the literature. They include deoxyxylulose 5-phosphate synthase (DXS) and PSY, the rate-determining enzymes of the MEP and carotenoid pathways, respectively (Walter et al., 2015). Both DXS and PSY are encoded by single genes in Arabidopsis but several differentially expressed genes in tomato. Subfunctionalization is also widespread beyond the isoprenoid pathway, contributing to the huge diversity of specialized metabolism in plants (Moghe and Last, 2015). Deciphering how different plants regulate plastidial GGPP production and channeling will be useful for future metabolic engineering approaches targeted to manipulate the

accumulation of specific groups of GGPP-derived isoprenoids without negatively impacting the levels of others.

ACKNOWLEDGEMENTS

We greatly thank Juan Antonio López-Ráez for providing cDNA samples of non-mycorrhized and mycorrhized tomato roots; Ernesto Llamas for providing the pGWB417_AtPRK construct, and Albert Ferrer and Laura Gutiérrez for the pDE-Cas9 (with kanamycin resistance) plasmid. The technical support of M. Rosa Rodríguez-Goberna and all CRAG services is also appreciated. This work was funded by the European Regional Development Fund (FEDER) and the Spanish Agencia Estatal de Investigación (grants BIO2017-84041-P and, BIO2017-90877-REDT) and Generalitat de Catalunya (2017SGR-710) to MRC. Support by the collaborative European Union's Horizon 2020 (EU-H2020) ERA-IB-2 (Industrial Biotechnology) BioProMo project to MRC (PCIN-2015-103), RK and JB (053-80-725) is also acknowledged. CRAG is financially supported by the Severo Ochoa Programme for Centres of Excellence in R&D 2016-2019 (SEV-2015-0533) and the Generalitat de Catalunya CERCA Programme. MVB was funded with a Spanish Ministry of Education, Culture and Sports PhD fellowship (FPU14/05142) and a EU-H2020 COST Action CA15136 (EuroCaroten) short-stay fellowship. ME is supported by a Spanish Agencia Estatal de Investigación (BES-2017-080652) PhD fellowship. IFS is supported by the EU-H2020 Marie S. Curie Action 753301 (Arcatom).

AUTHOR CONTRIBUTIONS

MVB, ME and MRC designed the research; MVB, ME, SB, GD, IFS, EF, and AF performed research; RK, ARF and JB contributed analytic tools; MVB, ME, SB, GD, IFS, EF, AF, RK, ARF, JB and MRC analyzed data; MVB and MRC wrote the paper. MVB and ME contributed equally to this work.

REFERENCES

Ahrazem, O., Argandoña, J., Fiore, A., Aguado, C., Luján, R., Rubio-Moraga, Á., Marro, M., Araujo-Andrade, C., Loza-Alvarez, P., Diretto, G., and Gómez-Gómez, L. (2018). Transcriptome analysis in tissue sectors with contrasting crocins accumulation provides novel insights into apocarotenoid biosynthesis and regulation during chromoplast biogenesis. Sci. Rep. 8: 1–17.

Ament, K., Van Schie, C.C., Bouwmeester, H.J., Haring, M.A., and Schuurink, R.C. (2006). Induction of a leaf specific geranylgeranyl pyrophosphate synthase and emission of (E,E)-4,8,12-trimethyltrideca-1,3,7,11-tetraene in tomato are dependent on both jasmonic acid and salicylic acid signaling pathways. Planta 224: 1197–1208.

Araújo, W.L., Tohge, T., Ishizaki, K., Leaver, C.J., and Fernie, A.R. (2011). Protein degradation - an alternative respiratory substrate for stressed plants. Trends Plant Sci. 16: 489–498.

Barja, M.V. and Rodríguez-Concepción, M. (2020). A Simple In Vitro Assay to Measure the Activity of Geranylgeranyl Diphosphate Synthase and Other Short-Chain Prenyltransferases. Methods Mol. Biol. 2083: 27–38.

Bartley, G. and Scolnik, P. (1993). cDNA Cloning, Expression during Development, and Genome Mapping of a second phytoenen synthase. Biochemistry 268: 25718–25721.

Bartley, G.E., Viitanen, P. V, Bacot, K.O., and Scolnik, P.A. (1992). A tomato gene expressed during fruit ripening encodes an enzyme of the carotenoid biosynthesis pathway. J. Biol. Chem. 267: 5036–9.

Baslam, M., Esteban, R., García-Plazaola, J.I., and Goicoechea, N. (2013). Effectiveness of arbuscular mycorrhizal fungi (AMF) for inducing the accumulation of major carotenoids, chlorophylls and tocopherol in green and red leaf lettuces. Appl. Microbiol. Biotechnol. 97: 3119–3128.

Beck, G., Coman, D., Herren, E., Ruiz-Sola, M.A., Rodríguez-Concepción, M., Gruissem, W., and Vranová, E. (2013). Characterization of the GGPP synthase gene family in *Arabidopsis thaliana*. Plant Mol. Biol. 82: 393–416.

Bradford, M.M. (1976). A rapid and sensitive method for the quantitation of microgram quantities of protein utilizing the principle of protein-dye binding. Anal. Biochem. 72: 248–54.

Camagna, M., Grundmann, A., Bär, C., Koschmieder, J., Beyer, P., and Welsch, R. (2019). Enzyme Fusion Removes Competition for Geranylgeranyl Diphosphate in Carotenogenesis. Plant Physiol. 179: 1013–1027.

Camara, B. (1993). Plant phytoene synthase complex: Component enzymes, Immunology and Biogenesis. Methods Enzymol. 214: 352–365.

D'Andrea, L., Simon-Moya, M., Llorente, B., Llamas, E., Marro, M., Loza-Alvarez, P., Li, L., and Rodriguez-Concepcion, M. (2018). Interference with Clp protease impairs carotenoid accumulation during tomato fruit ripening. J. Exp. Bot. 69: 1557–1568.

Diretto, G., Frusciante, S., Fabbri, C., Schauer, N., Busta, L., Wang, Z., Matas, A.J., Fiore, A.,

Rose J.K.C., Fernie, A.R. et al. (2020). Manipulation of β-carotene levels in tomato fruits results in increased ABA content and extended shelf life. Plant Biotechnol. J. 18: 1185–1199.

Dogbo, O. and Camara, B. (1987). Purification of isopentenyl pyrophosphate isomerase and geranylgeranyl pyrophosphate synthase from *Capsicum* chromoplasts by affinity chromatography. Biochim. Biophys. Acta (BBA)/Lipids Lipid Metab. 920: 140–148.

Estornell, L.H., Orzáez, D., López-Peña, L., Pineda, B., Antón, M.T., Moreno, V., and Granell, A. (2009). A multisite gateway-based toolkit for targeted gene expression and hairpin RNA silencing in tomato fruits. Plant Biotechnol. J. 7: 298–309.

Fernandez, A.I., Viron, N., Alhagdow, M., Karimi, M., Jones, M., Amsellem, Z., Sicard, A., Czerednik, A., Angenent, G., Grierson, D. et al. (2009). Flexible Tools for Gene Expression and Silencing in Tomato. Plant Physiol. 151: 1729–1740.

Fester, T., Schmidt, D., Lohse, S., Walter, M.H., Giuliano, G., Bramley, P.M., Fraser, P.D., Hause, B., and Strack, D. (2002). Stimulation of carotenoid metabolism in arbuscular mycorrhizal roots. Planta 216: 148–154.

Fester, T., Wray, V., Nimtz, M., and Strack, D. (2005). Is stimulation of carotenoid biosynthesis in arbuscular mycorrhizal roots a general phenomenon? Phytochemistry 66: 1781–1786.

Fraser, P.D., Enfissi, E.M.A., Halket, J.M., Truesdale, M.R., Yu, D., Gerrish, C., and Bramley, P.M. (2007). Manipulation of Phytoene Levels in Tomato Fruit: Effects on Isoprenoids, Plastids, and Intermediary Metabolism. Plant Cell 19: 3194–3211.

Fraser, P.D., Romer, S., Shipton, C.A., Mills, P.B., Kiano, J.W., Misawa, N., Drake, R.G., Schuch, W., and Bramley, P.M. (2002). Evaluation of transgenic tomato plants expressing an additional phytoene synthase in a fruit-specific manner. Proc. Natl. Acad. Sci. U. S. A. 99: 1092–7.

Fraser, P.D., Schuch, W., and Bramley, P.M. (2000). Phytoene synthase from tomato (*Lycopersicon esculentum*) chloroplasts--partial purification and biochemical properties. Planta 211: 361–369.

Fray, R.G. and Grierson, D. (1993). Identification and genetic analysis of normal and mutant phytoene synthase genes of tomato by sequencing, complementation and co-suppression. Plant Mol. Biol. 22: 589–602.

Fujisawa, M., Nakano, T., Shima, Y., and Ito, Y. (2013). A large-scale identification of direct targets of the tomato MADS box transcription factor RIPENING INHIBITOR reveals the regulation of fruit ripening. Plant Cell 25: 371–386.

Fujisawa, M., Shima, Y., Nakagawa, H., Kitagawa, M., Kimbara, J., Nakano, T., Kasumi, T., and

Ito, Y. (2014). Transcriptional regulation of fruit ripening by tomato FRUITFULL homologs and associated MADS box proteins. Plant Cell 26: 89–101.

Galili, G., Amir, R., and Fernie, A.R. (2016). The Regulation of Essential Amino Acid Synthesis and Accumulation in Plants. Annu. Rev. Plant Biol. 67: 153–178.

Giorio, G., Stigliani, A.L., and D'Ambrosio, C. (2008). Phytoene synthase genes in tomato (Solanumlycopersicum L.) - New data on the structures, the deduced amino acid sequences and the expression patterns. FEBS J. 275: 527–535.

Gonzalo, M.J., Brewer, M.T., Anderson, C., Sullivan, D., Gray, S., and Van Der Knaap, E. (2009). Tomato fruit shape analysis using morphometric and morphology attributes implemented in tomato analyzer software program. J. Am. Soc. Hortic. Sci. 134: 77–87.

Goytia, E., Fernández-Calvino, L., Martínez-García, B., López-Abella, D., and López-Moya, J.J. (2006). Production of plum pox virus HC-Pro functionally active for aphid transmission in a transient-expression system. J. Gen. Virol. 87: 3413–23.

Höhner, R., Aboukila, A., Kunz, H.-H., and Venema, K. (2016). Proton Gradients and Proton-Dependent Transport Processes in the Chloroplast. Front. Plant Sci. 7: 1–7.

Kachanovsky, D.E., Filler, S., Isaacson, T., and Hirschberg, J. (2012). Epistasis in tomato color mutations involves regulation of phytoene synthase 1 expression by *cis*-carotenoids. Proc. Natl. Acad. Sci. U. S. A. 109: 19021–6.

Liu, H., Ding, Y., Zhou, Y., Jin, W., Xie, K., and Chen, L.L. (2017). CRISPR-P 2.0: An Improved CRISPR-Cas9 Tool for Genome Editing in Plants. Mol. Plant 10: 530–532.

Llorente, B., D'Andrea, L., Ruiz-Sola, M.A., Botterweg, E., Pulido, P., Andilla, J., Loza-Alvarez, P., and Rodriguez-Concepcion, M. (2016). Tomato fruit carotenoid biosynthesis is adjusted to actual ripening progression by a light-dependent mechanism. Plant J. 85: 107–19.

Llorente, B., Torres-Montilla, S., Morelli, L., Florez-Sarasa, I., Matus, J.T., Ezquerro, M., D'Andrea, L., Houhou, F., Majer, E., Picó, B. et al. (2020) Synthetic conversion of leaf chloroplasts into carotenoid-rich plastids reveals mechanistic basis of natural chromoplast development. Proc. Natl. Acad. Sci. USA 117: 21796-803.

Maudinas, B., Bucholtz, M.L., Papastephanou, C., Katiyar, S.S., Briedis, A. V., and Porter, J.W. (1977). The partial purification and properties of a phytoene synthesizing enzyme system. Arch. Biochem. Biophys. 180: 354–362.

McQuinn, R.P., Gapper, N.E., Gray, A.G., Zhong, S., Tohge, T., Fei, Z., Fernie, A.R., and Giovannoni, J.J. (2020). Manipulation of ZDS in tomato exposes carotenoid- and ABA-specific

effects on fruit development and ripening. Plant Biotechnol. J. 18: 2210-2224.

Moghe, G.D. and Last, R.L. (2015). Something Old, Something New: Conserved Enzymes and the Evolution of Novelty in Plant Specialized Metabolism. Plant Physiol. 169: 1512–1523.

Muñoz, A. and Castellano, M.M. (2018). Coimmunoprecipitation of Interacting Proteins in Plants. Methods Mol. Biol. 1794: 279–287.

Muñoz, P. and Munné-Bosch, S. (2018). Photo-oxidative stress during leaf, flower and fruit development. Plant Physiol. 176: 1004–1014.

Nagel, R., Bernholz, C., Vranová, E., Košuth, J., Bergau, N., Ludwig, S., Wessjohann, L., Gershenzon, J., Tissier, A., and Schmidt, A. (2015). *Arabidopsis thaliana* isoprenyl diphosphate synthases produce the C 25 intermediate, geranylfarnesyl diphosphate. Plant J. 84: 847–859.

Nisar, N., Li, L., Lu, S., Khin, N.C., and Pogson, B.J. (2015). Carotenoid metabolism in plants. Mol. Plant 8: 68–82.

Obata, T. and Fernie, A.R. (2012). The use of metabolomics to dissect plant responses to abiotic stresses. Cell. Mol. Life Sci. 69: 3225–3243.

Okada, K., Saito, T., Nakagawa, T., Kawamukai, M., and Kamiya, Y. (2000). Five geranylgeranyl diphosphate synthases expressed in different organs are localized into three subcellular compartments in Arabidopsis. Plant Physiol. 122: 1045–1056.

Orlova, I., Nagegowda, D.A., Kish, C.M., Gutensohn, M., Maeda, H., Varbanova, M., Fridman, E., Yamaguchi, S., Hanada, A., Kamiya, Y. et al. (2009). The small subunit of snapdragon geranyl diphosphate synthase modifies the chain length specificity of tobacco geranylgeranyl diphosphate synthase in planta. Plant Cell 21: 4002–4017.

Pulido, P., Perello, C., and Rodriguez-Concepcion, M. (2012). New Insights into Plant Isoprenoid Metabolism. Mol. Plant 5: 964–967.

Pulido, P., Toledo-Ortiz, G., Phillips, M. a, Wright, L.P., and Rodríguez-Concepción, M. (2013). Arabidopsis J-protein J20 delivers the first enzyme of the plastidial isoprenoid pathway to protein quality control. Plant Cell 25: 4183–4194.

Quinet, M., Angosto, T., Yuste-Lisbona, F.J., Blanchard-Gros, R., Bigot, S., Martinez, J.P., and Lutts, S. (2019). Tomato Fruit Development and Metabolism. Front. Plant Sci. 10: 1554.

Rodriguez-Concepcion, M., Avalos, J., Bonet, M.L., Boronat, A., Gomez-Gomez, L., Hornero-Mendez, D., Limon, M.C., Meléndez-Martínez, A.J., Olmedilla-Alonso, B., Palou, A. et al. (2018). A global perspective on carotenoids: Metabolism, biotechnology, and benefits for

nutrition and health. Prog. Lipid Res. 70: 62–93.

Rodríguez-Concepción, M. and Boronat, A. (2015). Breaking new ground in the regulation of the early steps of plant isoprenoid biosynthesis. Curr. Opin. Plant Biol. 25: 17–22.

Ruiz-Lozano, J.M., Aroca, R., Zamarreño, Á.M., Molina, S., Andreo-Jiménez, B., Porcel, R., García-Mina, J.M., Ruyter-Spira, C., and López-Ráez, J.A. (2016). Arbuscular mycorrhizal symbiosis induces strigolactone biosynthesis under drought and improves drought tolerance in lettuce and tomato. Plant, Cell Environ. 39: 441–452.

Ruiz-Sola, M.Á., Coman, D., Beck, G., Barja, M.V., Colinas, M., Graf, A., Welsch, R., Rütimann, P., Bühlmann, P., Bigler, L. et al. (2016a). Arabidopsis GERANYLGERANYL DIPHOSPHATE SYNTHASE 11 is a hub isozyme required for the production of most photosynthesis-related isoprenoids. New Phytol. 209: 252–264.

Ruiz-Sola, M.Á., Barja, M.V., Manzano, D., Llorente, B., Schipper, B., Beekwilder, J., and Rodriguez-Concepcion, M. (2016b). A Single Arabidopsis Gene Encodes Two Differentially Targeted Geranylgeranyl Diphosphate Synthase Isoforms. Plant Physiol. 172: 1393–1402.

Ruiz-Sola, M.Á. and Rodríguez-Concepción, M. (2012). Carotenoid Biosynthesis in Arabidopsis: A Colorful Pathway. Arab. B. 10: e0158.

Sandmann, G. (2015). Carotenoids of Biotechnological Importance. Adv. Biochem. Eng. / Biotechnol. 148: 449–467.

Schiml, S., Fauser, F., and Puchta, H. (2016). CRISPR/Cas-Mediated Site-Specific Mutagenesis in *Arabidopsis thaliana* Using Cas9 Nucleases and Paired Nickases. Methods Mol. Biol. 1469: 111–122.

Seymour, G.B., Chapman, N.H., Chew, B.L., and Rose, J.K.C. (2013). Regulation of ripening and opportunities for control in tomato and other fruits. Plant Biotechnol. J. 11: 269–278.

Simon, P. (2003). Q-Gene: Processing quantitative real-time RT-PCR data. Bioinformatics 19: 1439–1440.

Sparkes, I.A., Runions, J., Kearns, A., and Hawes, C. (2006). Rapid, transient expression of fluorescent fusion proteins in tobacco plants and generation of stably transformed plants. Nat. Protoc. 1: 2019–25.

Stauder, R., Welsch, R., Camagna, M., Kohlen, W., Balcke, G.U., Tissier, A., and Walter, M.H. (2018). Strigolactone Levels in Dicot Roots Are Determined by an Ancestral Symbiosis-Regulated Clade of the PHYTOENE SYNTHASE Gene Family. Front. Plant Sci. 9: 255.

Sun, T., Yuan, H., Cao, H., Yazdani, M., Tadmor, Y., and Li, L. (2018). Carotenoid Metabolism in

Plants: The Role of Plastids. Mol. Plant 11: 58–74.

Tholl, D. (2015). Biosynthesis and Biological Functions of Terpenoids in Plants. Adv. Biochem. Eng. Biotechnol. 148: 63–106.

Vranová, E., Coman, D., and Gruissem, W. (2013). Network analysis of the MVA and MEP pathways for isoprenoid synthesis. Annu. Rev. Plant Biol. 64: 665–700.

Walter, M.H., Stauder, R., and Tissier, A. (2015). Evolution of root-specific carotenoid precursor pathways for apocarotenoid signal biogenesis. Plant Sci. 233: 1–10.

Wang, C., Chen, Q., Fan, D., Li, J., Wang, G., and Zhang, P. (2016). Structural Analyses of Short-Chain Prenyltransferases Identify an Evolutionarily Conserved GFPPS Clade in Brassicaceae Plants. Mol. Plant 9: 195–204.

Wang, G. and Dixon, R. a (2009). Heterodimeric geranyl(geranyl)diphosphate synthase from hop (*Humulus lupulus*) and the evolution of monoterpene biosynthesis. Proc. Natl. Acad. Sci. U. S. A. 106: 9914–9919.

Wang, J., Lin, H.-X., Su, P., Chen, T., Guo, J., Gao, W., and Huang, L.-Q. (2019). Molecular cloning and functional characterization of multiple geranylgeranyl pyrophosphate synthases (ApGGPPS) from *Andrographis paniculata*. Plant Cell Rep. 38: 117–128.

Wang, Q., Huang, X.-Q., Cao, T.-J., Zhuang, Z., Wang, R., and Lu, S. (2018). Heteromeric Geranylgeranyl Diphosphate Synthase Contributes to Carotenoid Biosynthesis in Ripening Fruits of Red Pepper (*Capsicum annuum var. conoides*). J. Agric. Food Chem. 66: 11691–11700.

Yuan, H., Zhang, J., Nageswaran, D., and Li, L. (2015). Carotenoid metabolism and regulation in horticultural crops. Hortic. Res. 2: 15036.

Zhang, M., Su, P., Zhou, Y.-J., Wang, X.-J., Zhao, Y.-J., Liu, Y.-J., Tong, Y.-R., Hu, T.-Y., Huang, L.-Q., and Gao, W. (2015). Identification of geranylgeranyl diphosphate synthase genes from *Tripterygium wilfordii*. Plant Cell Rep. 34: 2179–2188.

Zhang, M., Yuan, B., and Leng, P. (2009). The role of ABA in triggering ethylene biosynthesis and ripening of tomato fruit. J. Exp. Bot. 60: 1579–1588.

Zhou, F. and Pichersky, E. (2020). The complete functional characterisation of the terpene synthase family in tomato. New Phytol. 226: 1341-1360.

Zhou, F., Wang, C.-Y., Gutensohn, M., Jiang, L., Zhang, P., Zhang, D., Dudareva, N., and Lu, S. (2017). A recruiting protein of geranylgeranyl diphosphate synthase controls metabolic flux toward chlorophyll biosynthesis in rice. Proc. Natl. Acad. Sci. U. S. A. 114: 6866–6871.

Zhu, X.F., Suzuki, K., Okada, K., Tanaka, K., Nakagawa, T., Kawamukai, M., and Matsuda, K. (1997a). Cloning and functional expression of a novel geranylgeranyl pyrophosphate synthase gene from *Arabidopsis thaliana* in *Escherichia coli*. Plant Cell Physiol. 38: 357–61.

Zhu, X.F., Suzuki, K., Saito, T., Okada, K., Tanaka, K., Nakagawa, T., Matsuda, H., and Kawamukai, M. (1997b). Geranylgeranyl pyrophosphate synthase encoded by the newly isolated gene GGPS6 from *Arabidopsis thaliana* is localized in mitochondria. Plant Mol. Biol. 35: 331–41.

Zouine, M., Maza, E., Djari, A., Lauvernier, M., Frasse, P., Smouni, A., Pirrello, J., and Bouzayen, M. (2017). TomExpress, a unified tomato RNA-Seq platform for visualization of expression data, clustering and correlation networks. Plant J. 92: 727–735.

SUPPORTING INFORMATION

FIGURES

TABLES

Table S10. Relative levels of metabolites detected by GC-MS in samples from WT and mutant B+10 fruit.

Table S11. Parameters used for peak annotation in B+10 fruit.

METHODS

Method S1. Growth conditions, sample collection and phenotypic analyses.

Method S2. Constructs.

Method S3. RNA isolation and cDNA synthesis.

Method S4. GGPPS activity determination.

Method S5. Subcellular localization assays.

Method S6. Co-immunoprecipitation assays.

Method S7. Isoprenoid analysis.

TABLES

Table 1. Kinetic parameters of tomato plastidial GGPPS enzymes

	DMAPP (+100 µM IPP)		**IPP** (+100 µM DMAPP)	
	Km (µM)	Vmax (nmol•min^{-1}•mg^{-1})	Km (µM)	Vmax (nmol•min^{-1}•mg^{-1})
SlG1	31.82 ± 2.92	47.47 ± 1.40	74.18 ± 7.55	59.87 ± 2.73
SlG2	49.55 ± 5.31	38.87 ± 1.53	79.75 ± 8.33	36.73 ± 1.73
SlG3	45.75 ± 6.81	26.13 ± 1.40	45.92 ± 4.86	29.13 ± 1.13
AtG11	32.86 ± 4.86	21.53 ± 1.07	38.49 ± 4.94	24.13 ± 1.07

. Values correspond to the mean±SD of three independent experimental replicates (n=3).

Table 2. ABA levels in GGPPS-defective tomato leaves and fruit.

	Young leaves	B+10 fruit
WT	1.67 ± 0.19	0.63 ± 0.13
slg2-1	1.69 ± 0.10	0.55 ± 0.12
slg2-2	1.98 ± 0.39	**0.30 ± 0.08**
slg3-1	1.96 ± 0.09	**0.16 ± 0.04**
slg3-2	1.61 ± 0.29	**0.08 ± 0.01**

Values (µg/g dry weight) correspond to the mean ± SD of four independent samples (n=4). Statistically significant changes in mutants compared to WT samples (t-test, $p<0.01$) are indicated in bold.

Table 3. Expected and observed frequencies of the F2 population from the crosses of *slg2-2* and *slg3-1* mutant tomato plants.

		Round 1		Round 2		Combined	
Genotypes	Expected	#	%	#	%	#	%
G2g2 G3g3	25%	52	26%	15	20%	67	24%
G2g2 G3G3	12.5%	26	13%	18	24%	44	16%
G2G2 G3g3	12.5%	35	17.5%	10	13%	45	16%
g2g2 G3g3	12.5%	18	9%	6	8%	24	9%
G2g2 g3g3	12.5%	16	8%	5	7%	21	8%
g2g2 g3g3	6.25%	0	0%	0	0%	0	0%
g2g2 G3G3	6.25%	17	8.5%	5	7%	22	8%
G2G2 g3g3	6.25%	14	7%	8	11%	22	8%
G2G2 G3G3	6.25%	22	11%	9	12%	31	11%
Total plants (#)		200		76		276	
Chi-square			30.84		22.68		45.17
p-value			0.0002		0.0038		<0.0001

Mutant alleles are marked in red. A chi-squared goodness of fit test was performed with 8 degrees of freedom and 95% interval of confidence to check the Mendelian segregation of the mutant alleles. #, number of plants.

FIGURE LEGENDS

Figure 1. Gene co-expression analysis of tomato genes encoding plastidial GGPPS isoforms in leaf and fruit tissues. Positive co-expression relationships ($\rho \geq 0.55$) are depicted in tissue-specific networks as edges. *SlG1*, *SlG2* and *SlG3* are depicted as central green nodes. Surrounding smaller nodes represent genes from the indicated isoprenoid pathways. Red, green and black edges indicate positive co-expression with *SlG1, SlG2* and *SlG3* genes, respectively. See Table S4 for gene accessions, Table S5 for leaf and fruit datasets used, and Table S6 for ρ values.

Figure 2. Expression profiles of genes encoding tomato PSY and GGPPS paralogs during processes involving increased carotenoid production. First column corresponds to non-mycorrhized (-) and mycorrhized roots (+) at 6 weeks post-inoculation. Transcript levels were normalized using the tomato *EXP* gene and are shown relative to untreated root samples. Central column samples correspond to 7-day-old dark-grown seedlings at 0, 6 and 24 h after exposure to light and to seedlings continuously grown in the light (L). Transcript levels were normalized to the *EXP* gene and are represented relative to etiolated (0 h) samples. Third column depicts different fruit ripening stages: MG, mature green; B, breaker; O, orange; and R, red ripe. Levels were normalized using *ACT4* and are shown relative to MG samples. Expression values represent the mean±SD of three independent biological replicates (n=3). Asterisks indicate statistically significant differences relative to untreated (-), etiolated (0 h) or MG samples (t-test or one-way ANOVA with Dunnett's multiple comparisons test, *p<0.05, **p<0.01).

Figure 3. Co-immunoprecititation analyses. *Nicotiana benthamiana* leaves were co-agroinfiltrated with the indicated proteins tagged with C-terminal Myc (in blue) or HA (in red) epitopes. Controls agroinfiltrated only with the HA-tagged protein as indicated as (-). A fraction of the protein extracts (INPUT) was used to test protein production by immunoblot analyses using antibodies against Myc (αMyc) and HA (αHA). After immunoprecipitation (IP) of the remaining protein extracts using αMyc, samples were used for immunoblot analyses with αMyc (to confirm successful IP) and αHA (to detect the presence of co-immunoprecipitated HA-tagged proteins).

Figure 4. CRISPR-Cas9 mutagenesis of tomato *SlG2* and *SlG3* genes. (A) Scheme representing the designed strategy to generate deletions on *SlG2* and *SlG3* genes and the resulting proteins in selected mutant alleles (See Figures S6-S8 for further details). Green, pink and black boxes represent transit peptides, protein-protein interaction motifs, and catalytic domains (FARM and SARM), respectively. Blue arrowheads indicate the position of the designed sgRNAs encompassing specific restriction sites, and black arrows represent primer pairs used for

genotyping. **(B)** Activity assays of WT and mutant GGPPS enzymes in *E. coli* strains expressing bacterial genes for lycopene biosynthesis (*crtB* and *crtI*) but lacking GGPPS activity. Lycopene production after transformation with an empty vector (labelled as "Control" in the plots) or plasmid constructs harboring the indicated sequences is represented relative to the levels obtained with the bona-fide GGPPS enzyme AtG11. Values represent the mean±SD of at least three independent transformants (n=3).

Figure 5. Leaf phenotypes of mutant tomato lines defective in SlG2 or SlG3. (A) Representative images of 4-week-old plants of the indicated lines. **(B)** Relative levels of total carotenoids, chlorophylls and tocopherols in young and mature leaves of WT and mutant lines. Values are represented relative to WT levels and they correspond to the mean±SD of at least three independent biological replicates (n=3). See Table S7 for absolute values. **(C)** ϕPSII in young and mature leaves of the indicated lines. Values represent the mean±SD of four different leaf areas from three different plants. In all cases, different letters represent statistically significant differences ($p<0.05$) among means according to posthoc Tukey's tests run when one-way ANOVA detected different means.

Figure 6. Metabolic changes in *slg2* and *slg3* mutants. Colors represent statistically significant fold-change (FC) values (t-test, $p<0.05$) of metabolite levels in young leaves or ripe fruit (B+10) from mutant tomato plants relative to those in WT controls. Quantitative and technical data are detailed in Tables S8 and S9 for leaves and Tables S10 and S11 for fruit.

Figure 7. Flowering and fruit phenotypes of mutant tomato lines defective in SlG2 or SlG3. (A) Flowering time measured as days after germination (left) or number of leaves (right). Values correspond to the mean±SD of at least n=4 independent biological replicates. **(B)** Number of days to reach the indicated ripening stages represented as days post-anthesis on-vine (DPA, left) and days post-breaker off-vine (DPB, right). In both box-plots, the lower boundary of the boxes indicates the 25th percentile, the black line within the boxes marks the median, and the upper boundary of the boxes indicates the 75th percentile. Dots mark data values and whiskers above and below the boxes indicate the minimum and maximum values. **(C)** Representative images of fruit from WT and mutant lines harvested from the plant at the breaker stage. **(D)** Relative levels of individual carotenoids (phytoene, lycopene and **β**-carotene) and total tocopherols in B+10 fruits of WT and mutant lines. Values are represented relative to those in WT samples and correspond to the mean±SD of n=3 independent biological replicates. See Table S7 for absolute values. In all plots, different letters represent statistically significant differences (one-way ANOVA followed by Tukey's multiple comparisons test, $p<0.05$).

Figure 8. Leaf phenotypes of tomato lines with different combinations of *slg2* snd *slg3* mutations. (A) Representative images of 4-week-old plants of the indicated lines. Mutant alleles are marked in red. **(B)** Total levels of photosynthetic pigments (carotenoids and chlorophylls) in young and mature leaves of WT and mutant lines. Values, mean and SD of n=3 independent biological replicates are represented. **(C)** ϕPSII in young and mature leaves of the indicated lines. Values, mean and SD of four different leaf areas from three different plants are shown. In all plots, different letters represent statistically significant differences ($p<0.05$) among means according to posthoc Tukey's tests that were run once the existence of different means was established by one-way ANOVA.

Figure 9. Ripening-associated pigmentation and marker gene expression in tomato fruits with different combinations of *slg2* snd *slg3* mutations. (A) Average red color quantification (arbitrary units) of on-vine fruit from WT and mutant lines at the indicated times. Values represent the mean±SD of three different fruits (n=3) for each point. **(B)** RT-qPCR analysis of *ACS2* and *E8* transcript levels in WT and mutant fruits collected at the indicated developmental stages. Expression values were normalized using *ACT4* and represent the mean±SD of n=3 independent biological replicates. In all plots, asterisks indicate statistically significant differences among means relative to WT samples (t-test, *$p<0.05$, **$p<0.01$). Asterisk color represents the genotype.

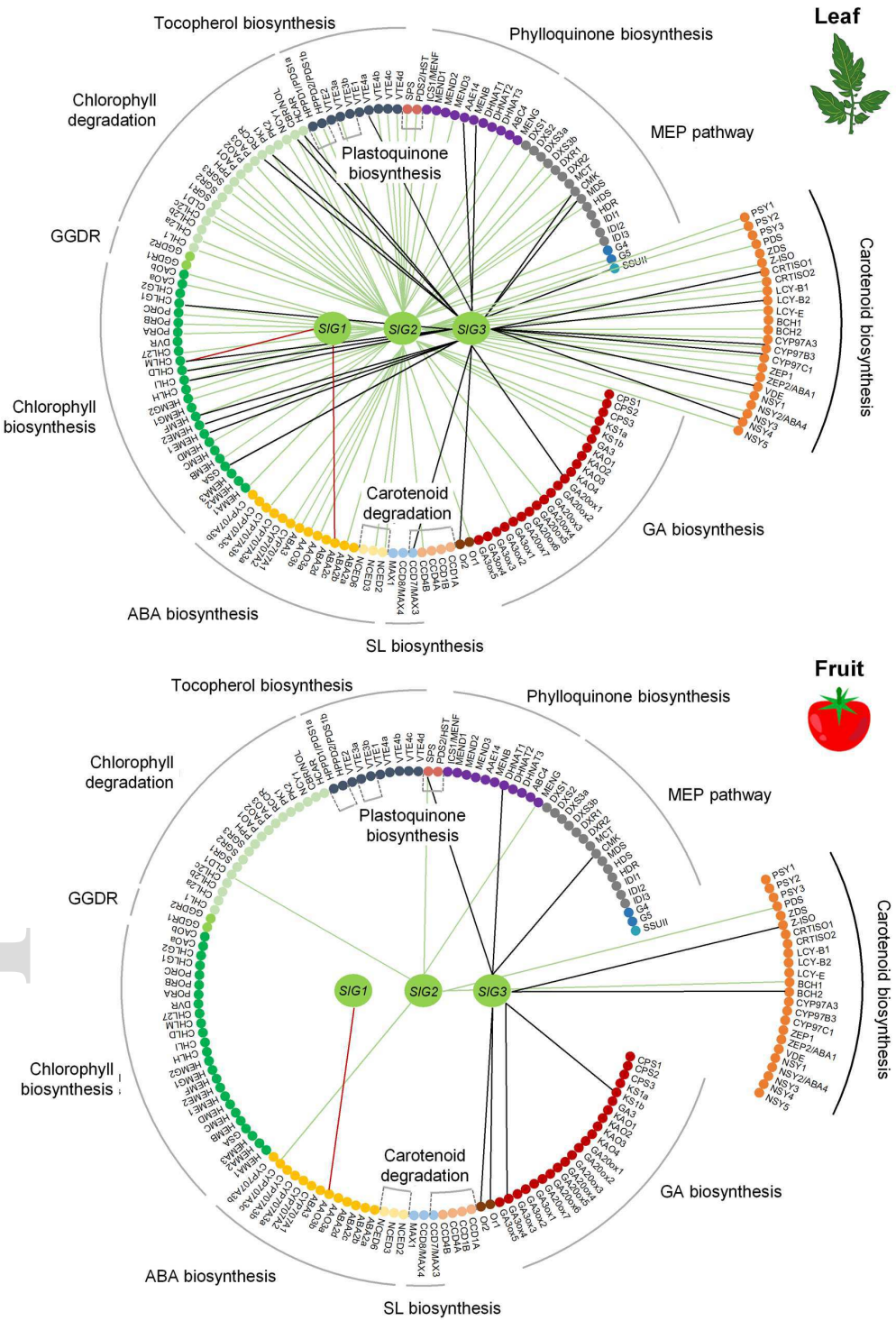

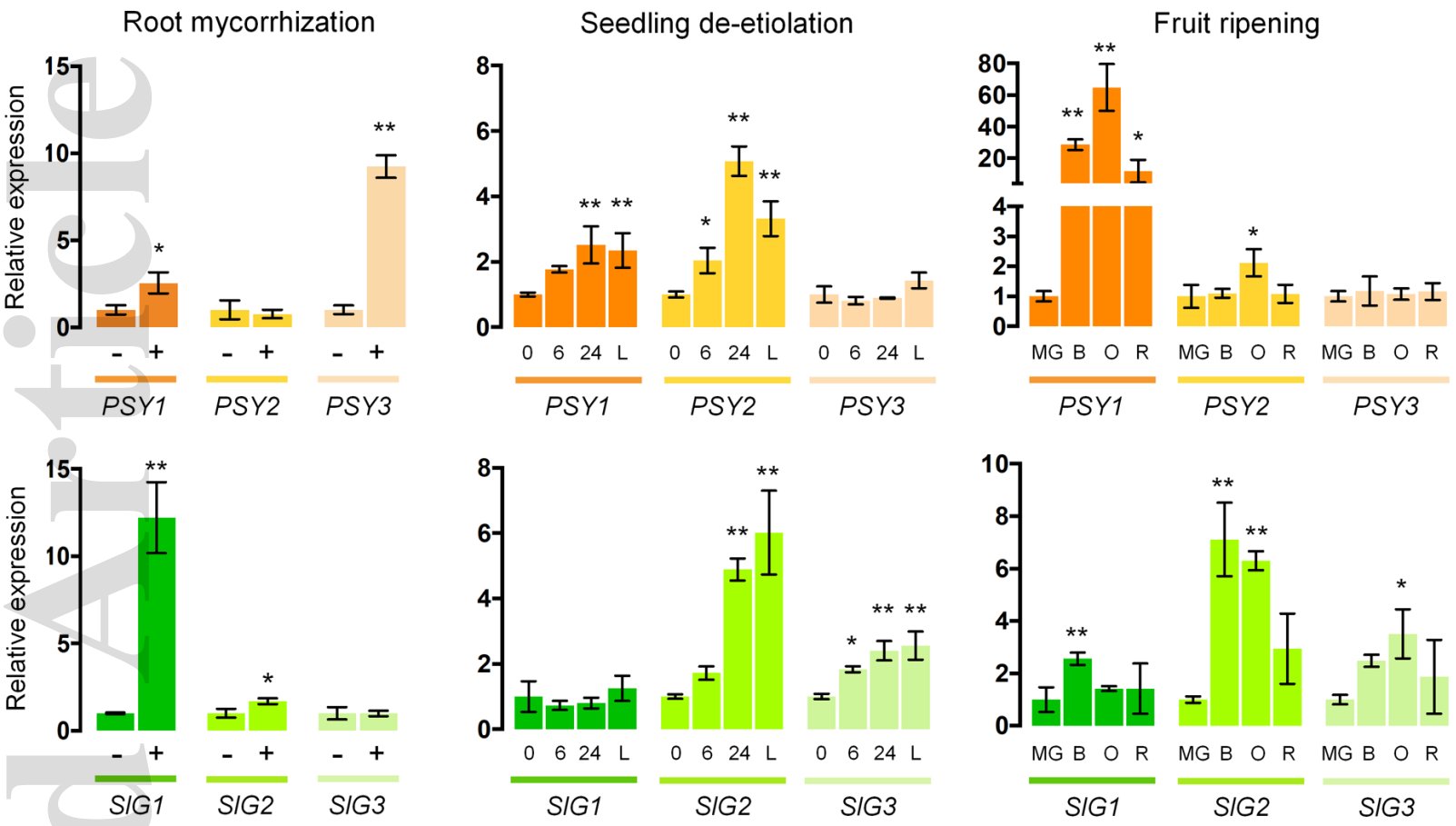

nph_17283_f2.eps

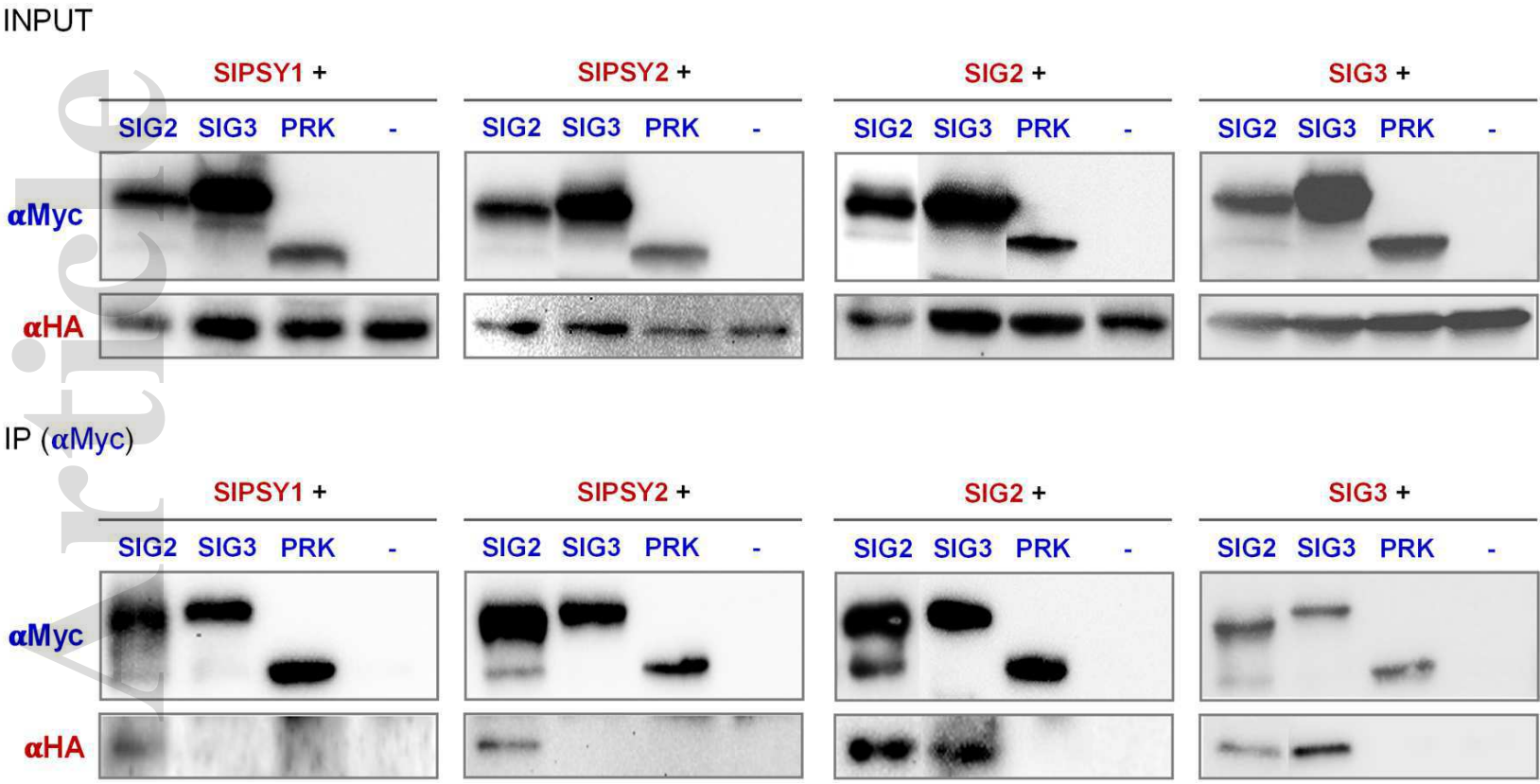

nph_17283_f3.eps

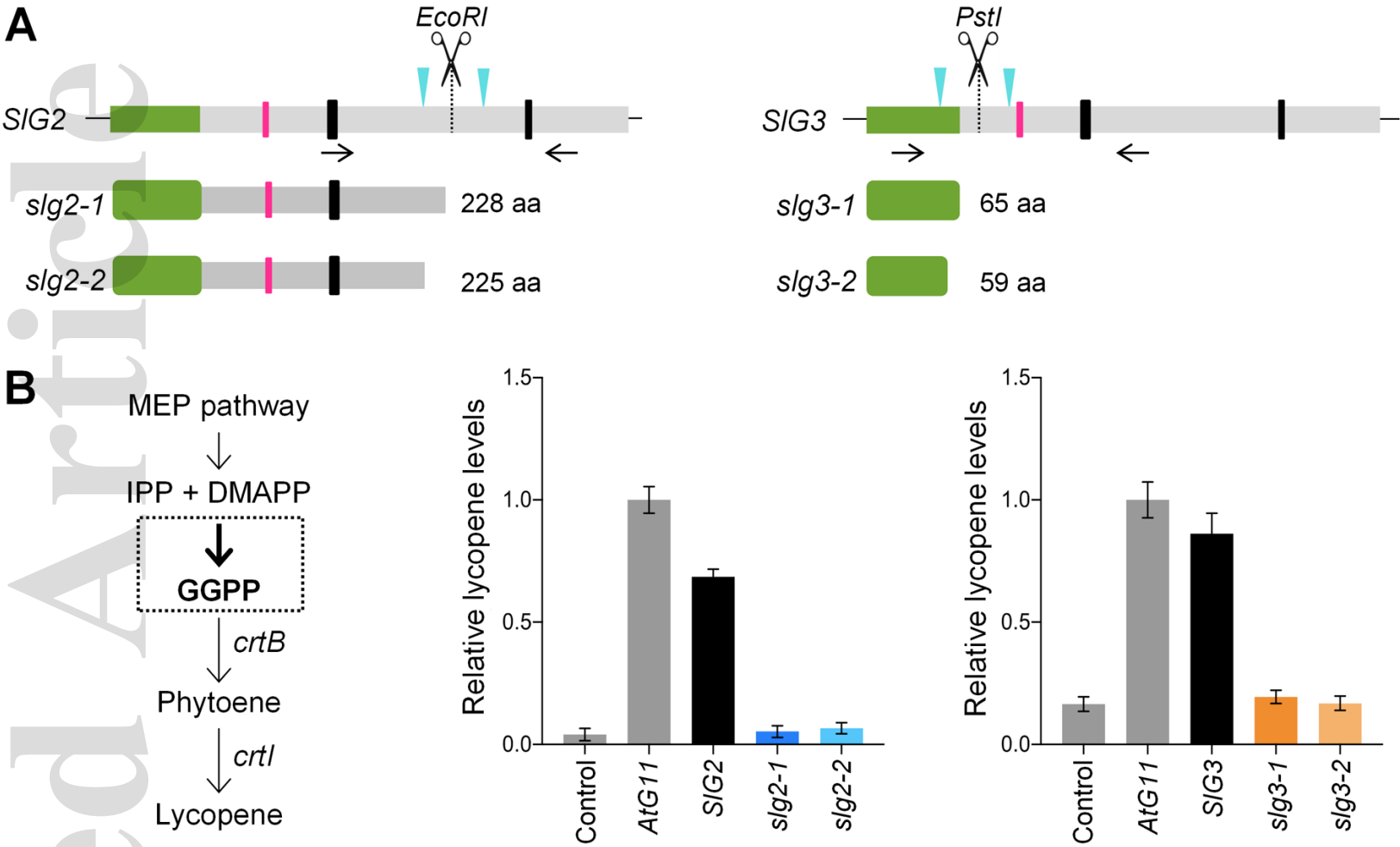

nph_17283_f4.eps

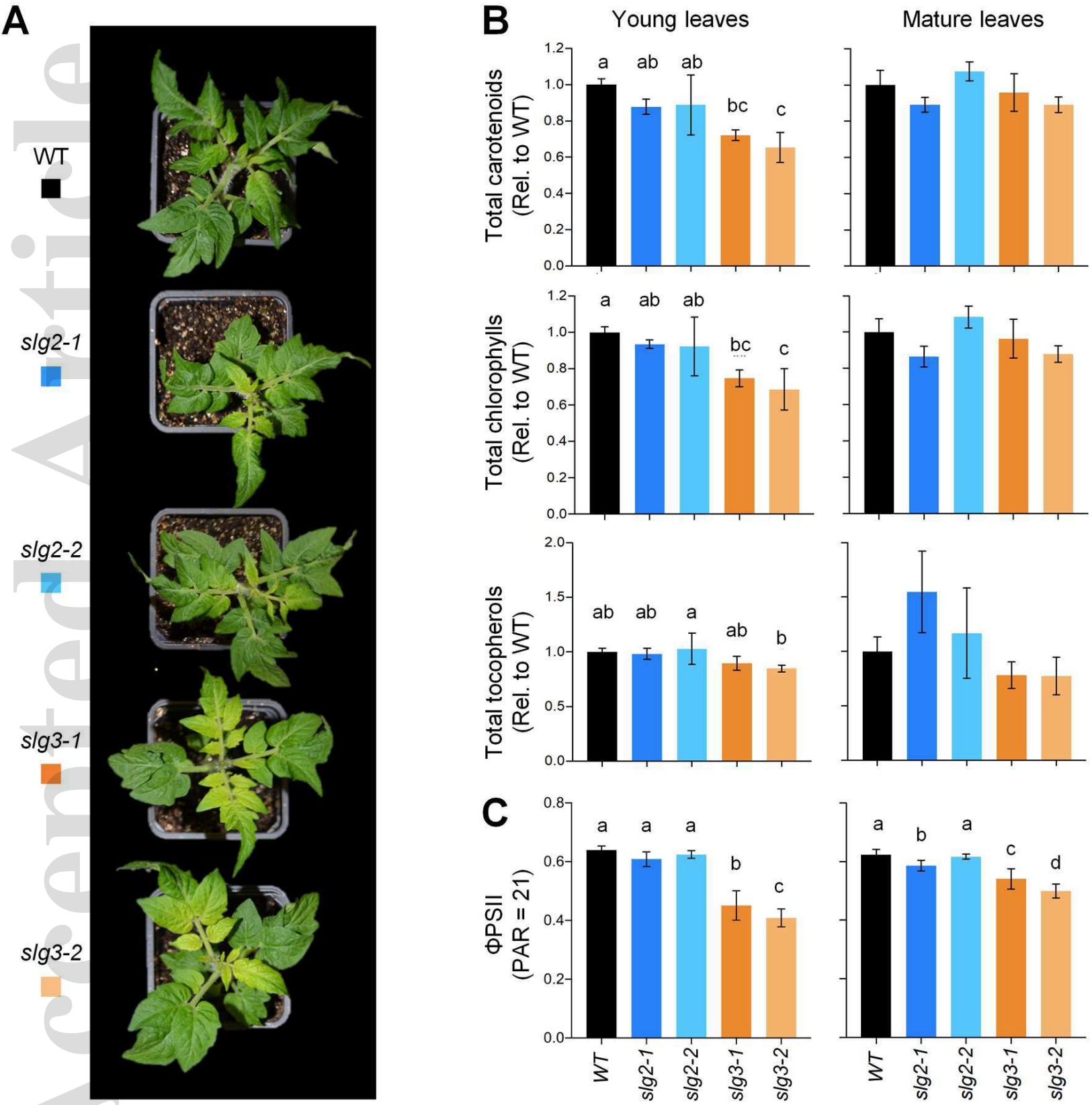

nph_17283_f5.eps

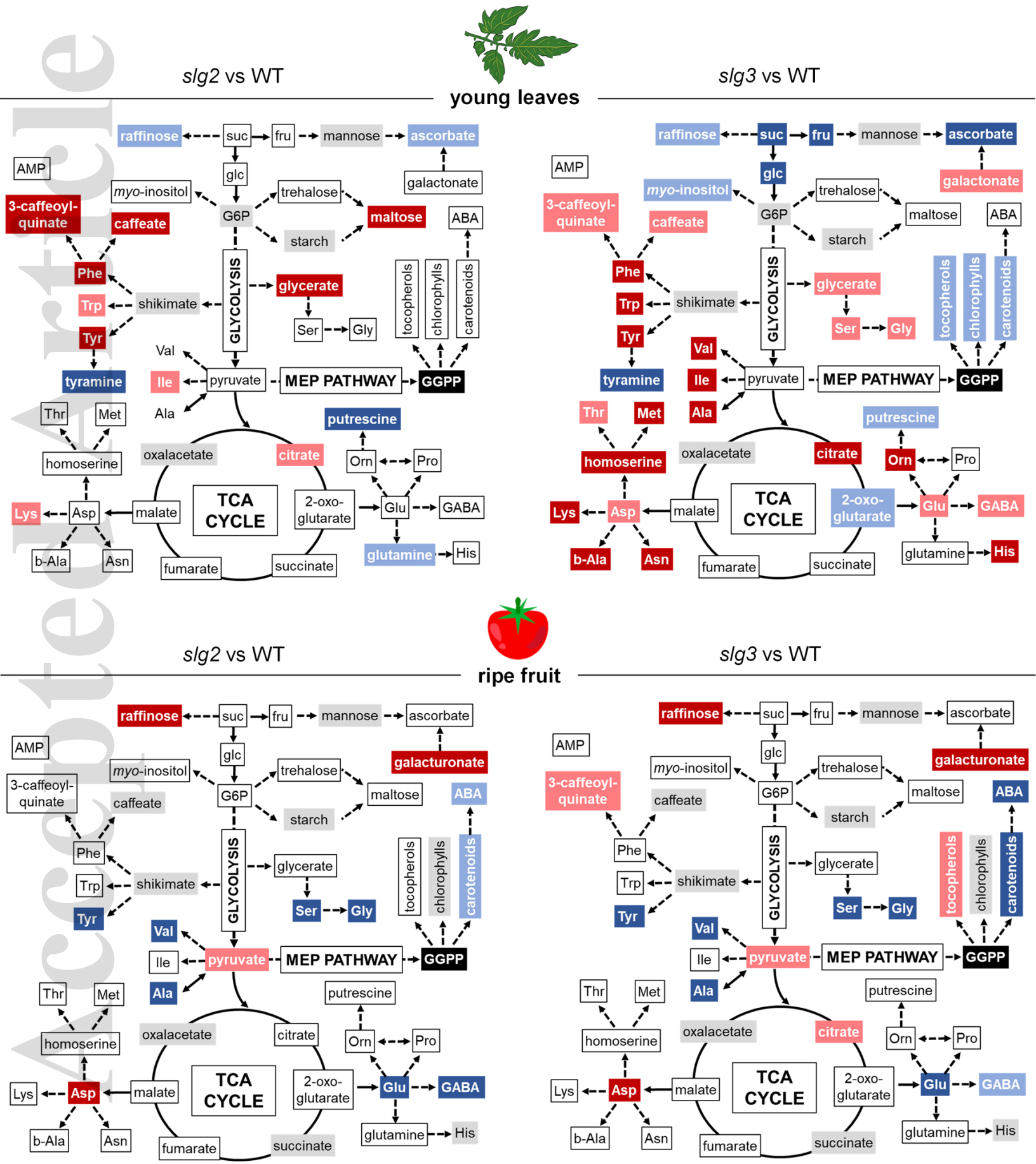

no change | UP FC < 2 | UP FC > 2 | DOWN FC < 2 | DOWN FC > 2 | not found

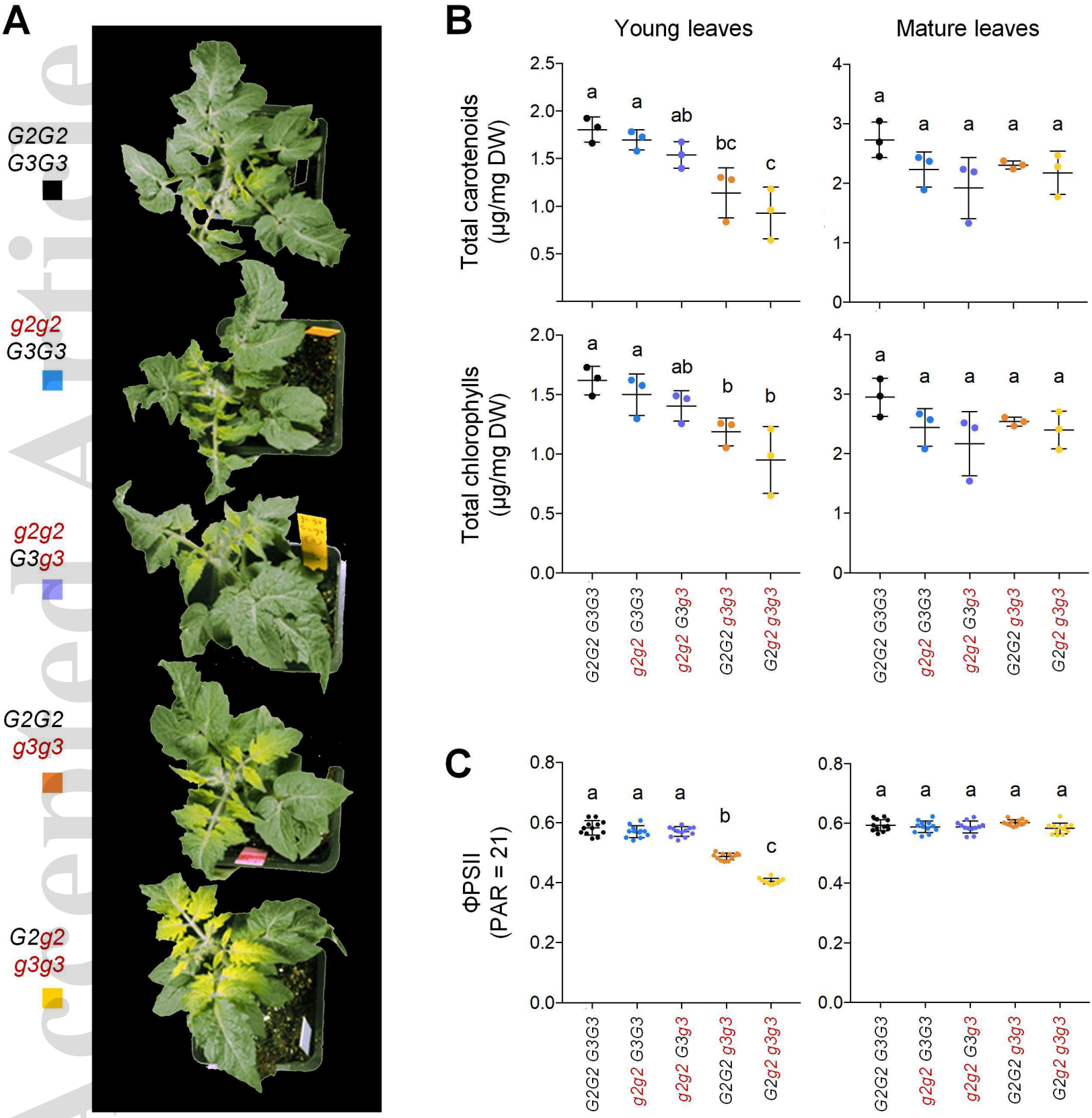

nph_17283_f7.eps

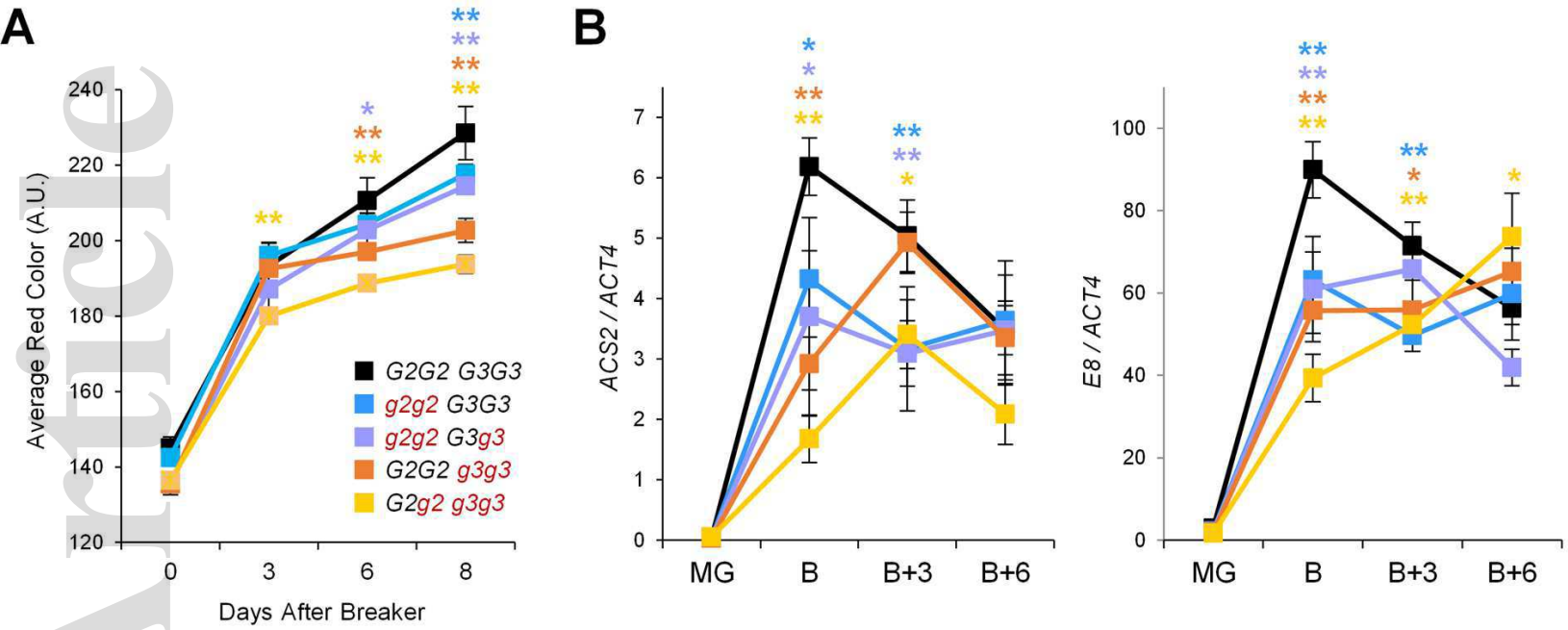

nph_17283_f9.eps